Assessing Functional and Structural Connectivity in Former Professional Athletes

ASSESSING FUNCTIONAL AND STRUCTURAL CONNECTIVITY IN FORMER PROFESSIONAL ATHLETES

BY

MITCHELL DOUGHTY, B.Eng.

A THESIS

SUBMITTED TO THE SCHOOL OF BIOMEDICAL ENGINEERING

AND THE SCHOOL OF GRADUATE STUDIES

OF MCMASTER UNIVERSITY

IN PARTIAL FULFILMENT OF THE REQUIREMENTS

FOR THE DEGREE OF

MASTER OF APPLIED SCIENCE

Master of Applied Science (2017) McMaster University

(School of Biomedical Engineering) Hamilton, Ontario, Canada

TITLE:	Assessing Functional and Structural Connectivity in Former Professional Athletes
AUTHOR:	Mitchell Doughty B.Eng., (Electrical and Biomedical Engineering) McMaster University, Hamilton, Canada
SUPERVISOR:	Dr. Michael Noseworthy
NUMBER OF PAGES:	xvi, 118

Lay Abstract

Sport-related concussions affect millions of athletes on a yearly basis in the United States alone. Concussions are often accompanied by short-lived neurological impairments, such as confusion, headaches, dizziness, nausea and memory loss. In addition, there is the potential for development of long term mental health and cognitive impairment. The goal of this work was to identify any neurological changes present in retired athletes of the Canadian Football League, through the use of advanced magnetic resonance imaging techniques evaluating thickness of brain structures, changes in brain activity, and alterations in core microstructure of the brain. Analyzing the results of these techniques revealed changes in a number of brain regions within the retired professional athlete population. These results suggest that a career of high impact sports may lead to short term, in addition to long-term neurological consequences.

Abstract

Recently there has been considerable attention directed towards the increased risk for head injuries that athletes face while participating in high impact sports. Furthermore, there is also heightened interest in the asymptomatic sport related subconcussive blows, commonly experienced during play, that possibly lead to long term neurological deficits. **Purpose**: The goal of this study was to investigate retired professional athletes of the Canadian Football League with a history of sport-related concussions, using several advanced MRI methods. The ultimate goal being the identification of any potential synergistic effects between a history of sport-related concussions, and exacerbated cognitive decline later on in life. **Materials and Methods**: Twenty former professional athletes of the Canadian Football League were scanned using a GE Discovery MR750 3T MRI with a 32-channel RF-coil. Axial FSPGR-3D images were used to define rs-BOLD and DTI scans. Seed based network analysis of the DMN was performed on rs-BOLD data. Voxel-wise tensor fitting of DTI data provided the means for estimating several tensor metrics. Results were normalized through comparison with a database of healthy controls. Potential associations between functional connectivity, white matter integrity, and cortical thickness measures were correlated with retired athlete position and years of professional play. **Results**: We found widespread cortical thinning in retired CFL subjects, alongside significant

increases in axial and mean diffusivity in the corona radiata and splenium and genu of the corpus callosum compared to controls. Seed based correlation analysis of the DMN network revealed interrupted connectivity in retired athletes. Athlete age, position, and number of years played appear to be factors in overall core white matter microstructural integrity. **Conclusions**: When compared to an age and sex matched control population, differences were observed both in functional and structural connectivity, suggesting that even years after retiring the brains of these former athletes still exhibit signs of damage.

Acknowledgements

I would like to thank my supervisor, Dr. Michael Noseworthy, for giving me the opportunity to further my knowledge in Biomedical Engineering, and explore a topic that I truly am passionate about. I would also like to thank Dr. John Connolly, along with Kyle Ruiter, and Rober Boshra who were invaluable resources in the completion of the CFL project. Further, I would like to acknowledge Steve Buist from the Hamilton Spectator, and his incredible contribution into organizing and completing this grand undertaking. I would also like to thank Norm Konyer for his help on understanding the technical aspects of MRI. I really appreciate all of the hard work and early mornings put in by the IRC technologists, Carol Awde, Cheryl Contant, and Julie Lecomte in order to complete the data collection process.

Last, but not least, a huge thank you to all of my labmates of past and present years; Alireza Akbari, Michael Behr, Caty Charles Herrera, Olga Dona Lemus, Dave Stillo, Amy Harrison, Evan McNabb, Conrad Rockel, Alejandro Santos Diaz, Saurabh Shaw, Nick Simard, and Diana Harasym. It has been a pleasure getting to know every one of you. Thanks for a fantastic two years!

Notation and abbreviations

AD	Axial diffusivity
BDI-II	Beck Depression Inventory II
BET	Brain extraction tool
CFL	Canadian Football League
CNS	Central nervous system
DMN	Default mode network
DTI	Diffusion tensor imaging
DWI	Diffusion weighted imaging
EEG	Electroencephalogram
EPI	Echo-planar imaging
FA	Fractional anisotropy
FT	Fourier Transform
GM	Grey matter
ImPACT	Immediate Post-Concussion Assessment and Cognitive Test
MD	Mean diffusivity
MRI	Magnetic Resonance Imaging
mTBI	Mild traumatic brain injury
PCSS	Post Concussion Symptom Scale

RD	Radial diffusivity
RF	Radio frequency
ROI	Region of interest
SF-36	Short-form Health Survey
T1	Spin-lattice relaxation time
T2	Spin-spin relaxation time
TBI	Traumatic brain injury
TE	Echo time
TR	Repetition time
WM	White matter

Contents

List of Figures

Chapter 1

Introduction

The work presented in this Masters thesis details the design and implementation of an analysis pipeline involving advanced magnetic resonance imaging (MRI) methods. The processes described will involve high level processing of MRI data, with the aim of evaluating functional, structural, and micro-structural integrity of white and grey matter in a group of former professional athletes of the Canadian Football League (CFL). The results of these detailed evaluations are presented at the end of the thesis, and offer insight into the damage potentially incurred through years of professional play. This chapter will serve as an introduction to the work, offering background information on the specifics of TBI and sport related concussion.

1.1 Understanding Concussion

In order to begin to describe the changes observed after a concussion, it is beneficial to begin with some background into the biological underpinnings of concussion. In a concussion, there frequently is severe impairment of neurological function post-injury.

However, these impairments do not always indicate the presence of macroscopic neural damage. Instead, these neurological impairments are a result of more minuscule changes in microstructural or functional characteristics of neural tissue (Giza and Hovda, 2014).

Functional connectivity will be referred to many times within this thesis. It can be described as any interruption of cellular or physiological function of the brain. Possible interruptions include any sort of metabolic change, disturbance in neurotransmission or ionic shift. Microstructural integrity will also be commonly referenced in this work. Microstructural integrity refers to any physical change to white matter tracts which is not readily observable through traditional clinical neuroimaging techniques (CT, standard MRI).

The neurobiology of concussion is incredibly complex, involving a series of events featuring bioenergetic deficits, alterations to axonal and cystoskeletal structures, interruptions to neurotransmission and the potential for cell death or chronic dysfunction (Barkhoudarian *et al.*, 2011; Sexton *et al.*, 2014). A brief overview of neuroanatomy will be presented, followed by a description into some of the changes observed as part of the neurometabolic cascade which follows a concussion.

1.1.1 Neuroanatomy

In order to begin to describe the complex structure and interactions of the central nervous system (CNS), it is beneficial to start on a microscopic level. The CNS which contains the brain and spinal cord, is composed of the following three main components:

- Neurons

- Glial cells
- Extra-cellular matrix

Glial cells function to maintain the healthy operation of neurons through offering structural support, forming myelin and supplying oxygen and nutrients. Extra-cellular matrix works to provide structural support and maintain inter-cellular communication. Neurons are the most significant cell in the CNS. Supporting cells, such as glial and extra-cellular matrix offer aid to neurons. Neurons are composed of a cell body, dendrites and an axon. The neuron cell is shown visually in figure 1.1.

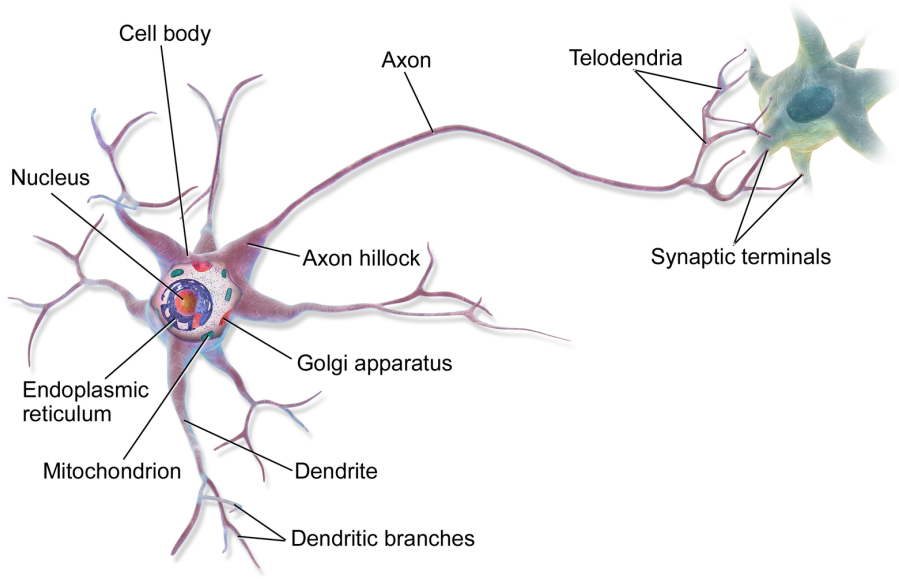

Figure 1.1: A multipolar neuron is shown. There are a large number of dendritic branches attached to the cell body, allowing for subsequent coordination and integration into a vast networks of neurons. By BruceBlaus (Own work) [CC BY 3.0 (http://creativecommons.org/licenses/by/3.0)], via Wikimedia Commons.

Neurons are designed specifically to take in information from the surroundings, process that information, and send it to other parts of the body in order to act upon it. Transmission of information between neurons occurs in the form of electro-chemical

events, through a process called neurotransmission (Hendelman, 2015). As shown in figure 1.1, the neuron cell has a cell body, dendrites which extend from the cell body, and an axon connecting one neuron with the others (through synaptic terminals).

Neurotransmission involves the movement of intra and extra-cellular fluids through ion channels along the axon of the neuron. These extra-cellular fluids each contain positively charged ions such as sodium (Na^+) and potassium (K^+), and negatively charged ions such as chloride (Cl^-) (Hendelman, 2015). The charge attached to ions and the concentration gradient across the intra and extra-cellular environment of the axon creates electrical charge across the neuronal membrane. This electrical charge is known as the resting potential of the axon, and is equal to roughly $-70mV$ in the CNS. In order for transmission of an electrical signal, a certain threshold of stimulation needs to be met. Once this threshold is met, the structure of the neuronal membrane allows for transmission of these electro-chemical messages down its length. Voltage and concentration-sensitive ion channels create voltage gradients across the axon. The dendrites (and cell body) of the next connecting neuron then receive this electro-chemical message, and proceed to transmit the firing pattern along the axon onto the next neuron. This occurs through the use of interneurons, which communicate through neurotransmitters at specialized synapse junctions.

The branched structure of neurons means that there are often thousands of inputs from other neurons at any one time, creating a vast and integrative network of neurons (Hendelman, 2015). Neurons which communicate amongst each other for a common purpose are frequently grouped together. Deep in the brain, these are referred to as nuclei. If they are grouped along the surface of the brain, they form what is called a cortex (Hendelman, 2015). Regions dense with neuron cells (cell bodies) are referred

to as grey matter.

The extending structure of axons allows them to reach across parts of the brain, connecting distant sections together. These axons are covered in a myelin sheath. The myelin coating is designed to enhance the speed of electro-chemical message transmission (Hendelman, 2015). Axons are also frequently grouped together into bundles of fibers, reaching from a cortex to nuclei, or vice versa, in order to transmit neuronal messages across the brain. These bundles of fibers are referred to as white matter, connecting various areas of grey matter within the brain.

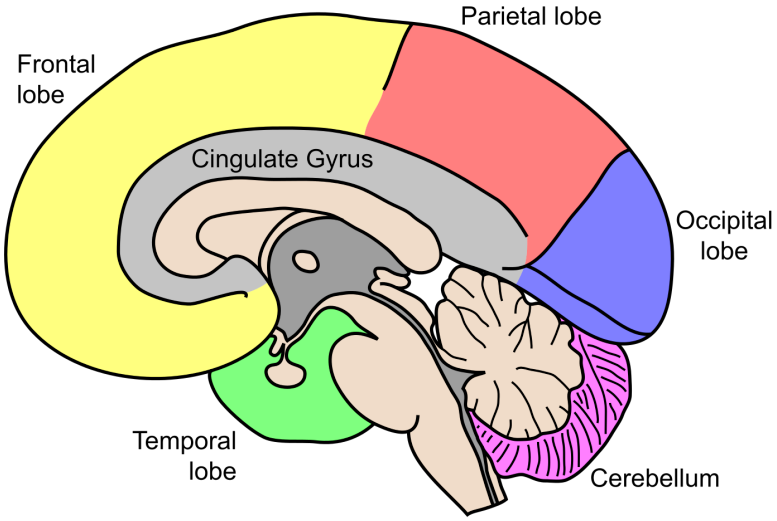

Figure 1.2: The lobes of the brain are shown visually. By NEUROtiker (Own work) [GFDL (http://www.gnu.org/copyleft/fdl.html), CC-BY-SA-3.0 (http://creativecommons.org/licenses/by-sa/3.0/) or CC BY-SA 2.5-2.0-1.0 (http://creativecommons.org/licenses/by-sa/2.5-2.0-1.0)], via Wikimedia Commons.

In figure 1.2, the basic lobes of the brain are shown. Each lobe is associated with a specific function. The frontal lobe is involved in short-term memory tasks, planning, motivation, and reward. The parietal lobe involves the processing of sensory information, as well as language. The occipital lobe is the central hub for visual

processing. The temporal lobe processes sensory input for association with emotion, and visual memory. The cingulate gyrus is involved in the limbic system, working to control emotion formation, learning and memory. The cerebellum serves as the region for coordinating muscle activity.

The white matter fiber structures described above work to connect different cortices, nuclei, or hemispheres within the brain. There are three main types of fiber structures or bundles:

- Commissural tracts
- Association tracts
- Projection tracts

Commissural tracts, the main tract being the corpus callosum, interconnect both hemispheres of the brain (also the anterior and posterior commissure, but these will not be discussed). The corpus callosum can be divided into three sections. The genu is the frontal portion, connecting left and right hemispheres of the frontal lobe. The body is the middle segment, connecting left and right wide areas of hemispheres. Finally, the splenium is the posterior portion, which connects left and right sections of the occipital lobe (Nowinski, 2011).

Association tracts connect different cortical regions within the same hemisphere. Association tracts include the longitudinal fasciculus (superior, middle, and inferior), occipito-frontal fasciculus (superior, and inferior), cingulum, and uncinate fasciculus. The superior longitudinal fasciculus and middle longitudinal fasciculus focus on connecting the frontal lobe with temporal, parietal and occipital lobes. The inferior longitudinal fasciculus interconnects the temporal lobe with the occipital lobe. The

optic-frontal fasciculus connects what it describes, the occipital and frontal lobes. The cingulum bundle connects sections of the temporal, parietal, and occipital lobes. Finally, the uncinate fasciculus links the frontal lobe with the temporal lobe (Nowinski, 2011).

Projection tracts involve connecting the cortex (outer layer) with subcortical structures in the diencephalon (thalamus, hypothalamus, and epithalamus), brainstem (midbrain, pons, and medulla oblongata) and spinal cord. These tracts include the corticospinal tract, corticothalamic tract, corticobulbar tract, and auditory radiations. The internal capsule, connecting the striatum and thalamus, is comprised of the corticothalamic tract, corticobulbar tract, and corticospinal tract. Fibers which diverge from the internal capsule form the corona radiata. The corona radiata connects to different regions in the cerebral cortex (Nowinski, 2011).

As we move forward in this thesis, specific regions of neuroanatomy identified in imaging analysis will be described in further detail if necessary.

1.1.2 Neurometabolic Cascade of Concussion

Now that we have some basic background on the delicate complexity of neuroanatomy, it is more feasible to get an appreciation for the potential damage a mild traumatic brain injury (mTBI) or concussion could impart on those structures. In the acute phase (hours to days post-injury) there are several different physiological processes at work, described as follows:

1. Ionic flux and glutamate release

2. Energy crisis

3. Cytoskeletal damage
4. Axonal dysfunction
5. Altered neurotransmission
6. Inflammation
7. Cell death

The overall physiological changes will be described, but specific detail into each individual step of the process is not necessary for understanding work in this thesis. Upon impact, there is an initial interruption of homeostasis within the cell, which initiates the related biochemical processes within the brain. Shearing and stretching forces of the biomechanical event can result in damage to the cell membranes of tissue, leading to the first stage of the cascade, an efflux of intracellular K^+ alongside influx of Na^+ and Ca^{2+} (MacFarlane and Glenn, 2015; Giza and Hovda, 2014). This exchange of ions results in hyperpolarization of the membrane, spreading across many neurons. In order to restore the altered ionic gradient environment, adenosine triphosphate (ATP) pumps are enacted (MacFarlane and Glenn, 2015; Giza and Hovda, 2014). This leads to a large consumption of ATP and subsequent state of increased metabolism. Hypermetabolism combined with decreased ATP supply can result in the energy crisis pointed to in stage two (MacFarlane and Glenn, 2015). Stage three, or impaired axonal function, is brought on through the increase in Ca^{+2} (from previously opened ligand-gated channels). Combining all of these significant metabolic disruptions, there arises the possibility for further, potentially long-term disruption including altered neurotransmission, inflammation and cell death.

Chapter 2

Background

This chapter will serve to provide a reasonable background on the imaging techniques utilized in this thesis. The description will begin by covering signal generation, then following into different methods of data reconstruction, and finally into using magnetic properties to probe different contrasts within the tissue.

2.1 Magnetic Resonance Imaging

MRI is a non-invasive imaging technique, involving a strong magnetic field and the use of radio frequency pulses in order to draw contrast and visualize tissue. During an MRI scan, subjects are situated within the bore of the magnet, and are exposed to a large homogeneous magnetic field, B_0, during the scan. Radio frequency (RF) pulses are used to alter local tissue characteristics and create signal contrast during the scan. Signal acquired from probing tissue through RF pulses is then digitized. Through a 2D Fourier transform, the data is reconstructed into a 2-dimensional image. These resultant 2-dimensional sliced images can be pieced together into a 3-dimensional

representation.

2.1.1 Signal Generation

MRI integrates three types of magnetic fields in order for proper operation. The first being the main homogeneous field, B_0. The second field is due to gradients, which are used for spatial localization of MRI signal. The final field involves RF pulses. RF pulses oscillate the magnetic field in order to alter local magnetic field properties of protons, offering the ability to extract tissue contrast.

The basic principle of MRI signal generation revolves around utilizing properties of protons in the body, mainly ^1H atoms, which are in great abundance in the body (in water and fat tissue). Hydrogen atoms possess a magnetic moment, and are randomly oriented within the body during daily processes. However, in the presence of a strong magnetic field (B_0), a small portion of the hydrogen spins will align with the magnetic field. This alignment in orientation creates a net magnetization of tissues within the body. The precessional frequency of the proton spins has been demonstrated to be proportional to the external magnetic field, and is given through the Larmor equation:

$$\omega_0 = \gamma B_0 \tag{2.1}$$

In the above equation, γ is a constant known as the gyromagnetic ratio. For protons, the gyromagnetic ratio is equal to $2.67x10^8 rad \cdot s^{-1}T^{-1}$. This equation offers the ability to calculate the frequency of precession for all nuclei in the magnetic field (in the absence of B_0 field inhomogeneities they all precess at the same rate).

2.1.2 Localization/K-space

Equation 2.1 offered a method of describing the spin precession of aligned nuclei, however, there is no way to produce an image with this information alone. This is due to a lack of spatial information. Spatial information would allow for the assignment of a location to each recorded signal, and ultimately, the creation of an image. Spatial localization is performed through the application of 3 orthogonal magnetic field gradients. During run time, gradients introduce spatial linear variability to the (normally fixed) B_0 field, in the Z direction (Bernstein *et al.*, 2004). The following set of equations describes the three orthogonal spatial gradients G_x, G_y, G_z.

$$G_x = \frac{\partial B_z}{\partial x},\ G_y = \frac{\partial B_z}{\partial y},\ G_z = \frac{\partial B_z}{\partial z} \tag{2.2}$$

Where G_x (or G_y, G_z) represents the linear gradient $\partial B_z/\partial x$, and z is the position along the z-axis. Using the above set of equations as reference, we can describe the overall magnetic field during gradient perturbation in the x direction as:

$$B(x) = B_0 + xG_x \tag{2.3}$$

We can then use the above equation to describe the effect of gradient action on the Larmor frequency. The updated Larmor equation including gradient contribution becomes:

$$\omega(x) = \gamma B(x) \tag{2.4}$$

In the above two equations, $B(x)$ is the linear gradient for the z direction. Computing gradient contributions in the y and z axis is as simple as substituting into Equation 2.3 for orthogonal directions.

We can then localize image slices through a combination of gradient information, RF transmit centre frequency and RF transmit bandwidth. At the isocentre of the magnet bore, the spins precess at the centre frequency of the transmitted RF (with no gradient contributions). Other regions away from the centre of the bore precess within a range defined by the RF transmit bandwidth.

The next step is to record signal from these precessing spins. Signal appears in the form of variable magnetic flux, which induces an electromotive force in the receiver coil through Faraday's law. The magnitude of current induced in the coil is dependent on the electromotive force (ε) and magnetic flux (ϕ_B) through the coil (Bernstein *et al.*, 2004). This relationship is described in the following equation:

$$\varepsilon = -\frac{d\phi_B}{dt} \tag{2.5}$$

In order to retrieve an image from the induced signal, a Fourier Transform (FT) operation is performed. First the raw spatial frequency information is read onto a grid-like space known as k-space. Outer regions of k-space contain high frequency information, which works to describe fine features in the final image. The centre regions of k-space contain low frequency information which work to define gross signal contrast of the image. Figure 2.1 visually demonstrates the reconstruction of k-space data into a finalized MR image.

There are many different techniques for traversing k-space. Some techniques aim to optimize reconstruction time, while others try to enhance scan quality. Sampling techniques include traditional techniques such as cartesian sampling, which occurs line by line. Other more complex techniques include spiral (circular trajectory moving

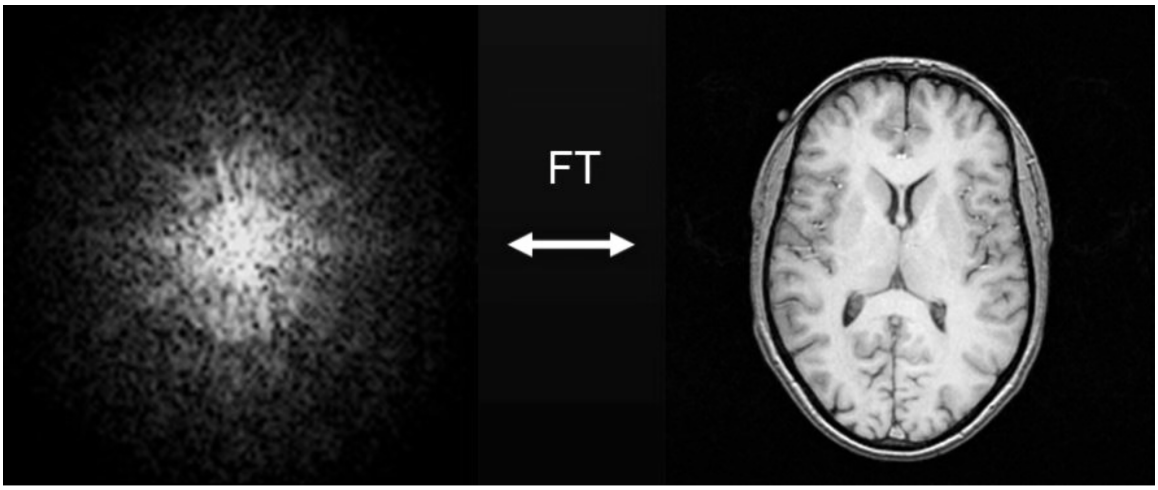

Figure 2.1: A visualization of k-space frequency data, and the resultant image after performing a 2D Fourier Transform operation. Image courtesy of Dr. Michael Noseworthy, McMaster University.

outward from the centre of k-space), radial (outward spokes from the centre of k-space) and echo planar imaging (right to left trajectory with a certain number of shots) techniques.

In the following chapters, the imaging methodology will be described in some detail. Two of the three performed imaging techniques, mainly diffusion weighted and Blood Oxygen Level-Dependant (BOLD) functional imaging, involve echo planar imaging (EPI) methods. EPI is an ultrafast acquisition technique, which obtains all of the necessary imaging data in a single echo. Bipolar readout and phase-encoding gradients are implemented in order to draw out a long train of gradient echoes. In figure 2.2, a visual representation of an RF pulse which uses EPI, along with the k-space trajectory, is given.

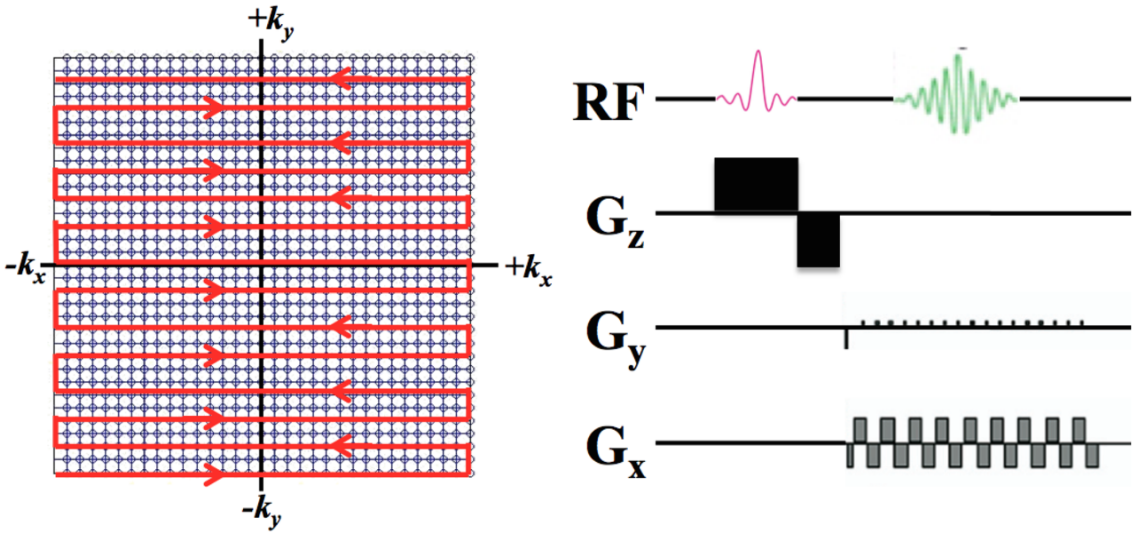

Figure 2.2: A visualization of k-space trajectory for an EPI sequence, and the accompanying pulse sequence diagram. Image courtesy of Dr. Michael Noseworthy, McMaster University.

2.1.3 Imaging Contrast

After the application of an RF pulse to excite protons within the B_0 field to flip spin precession into the transverse plane, the protons will begin to relax to their starting position. This relaxation can be broken down into two different mechanisms occurring simultaneously. The first involves a realignment of net magnetization back to the z-axis (parallel to B_0), and is coined longitudinal or spin-lattice T_1 relaxation. The second type of relaxation occurs during decay (or dephasing) of transverse components of magnetization, and is referred to as transverse or spin-spin T_2 relaxation.

The recovery of longitudinal magnetization follows an exponential growth curve, with T_1 as the time constant. T_1 changes with the strength of the main B_0 field, as well as the type of tissue being evaluated. For example, water has very long T_1 times (4000 msec), while the T_1 of fat is much shorter (250 ms). Recovery of transverse

magnetization follows an exponential decay, with time constant T_2. T_2 relaxation is a result of interaction of individual spins, leading to a loss of phase coherence with time (from differences in precessional frequencies). T_2 is not affected by the strength of the B_0 field, but instead is influenced by intrinsic properties of tissue.

A final imaging contrast to cover is referred to as T_2^*, which is a measure of signal decay. T_2^* is similar to T_2, however, it includes contributions due to inhomogeneities in the B_0 field, and tissue susceptibility. T_2^* is governed by the following equation:

$$\frac{1}{T_2^*} = \frac{1}{T_2} + \frac{1}{T_2'} \tag{2.6}$$

In the above equation $1/T_2'$ is a term related to the local inhomogeneity of the main B_0 field, and is equivalent to $\gamma \Delta B_0$ (also is dependent on field strength). T_2^* contrast is important in accentuating local magnetic homogeneity effects in tissue, and is utilized in BOLD functional imaging.

2.2 Diffusion Tensor Imaging

Diffusion weighted imaging (DWI) is an MR imaging technique focusing on the diffusion rate of water within tissue. Diffusion tensor imaging (DTI) builds on the information from DWI, providing a method to quantify the random Brownian diffusion of water, in the form of a tensor. The idea behind DTI lies in the ability to relate the measures of an estimated mathematical diffusion tensor to the structural integrity of white matter tissue within the brain. Prior work has demonstrated that white matter regions exhibit anisotropic tendencies, meaning that diffusion is restricted along a single, principal direction (along the white matter tract). In regions of grey matter,

however, there is more free diffusion occurring, with the tensor measure resembling that of less anisotropic diffusion. In regions of cerebrospinal fluid (CSF), there is completely unrestricted diffusion of water, and hence, the tensor measure is isotropic. Figure 2.3 visually demonstrates the differences between an isotropic and anisotropic diffusion tensor.

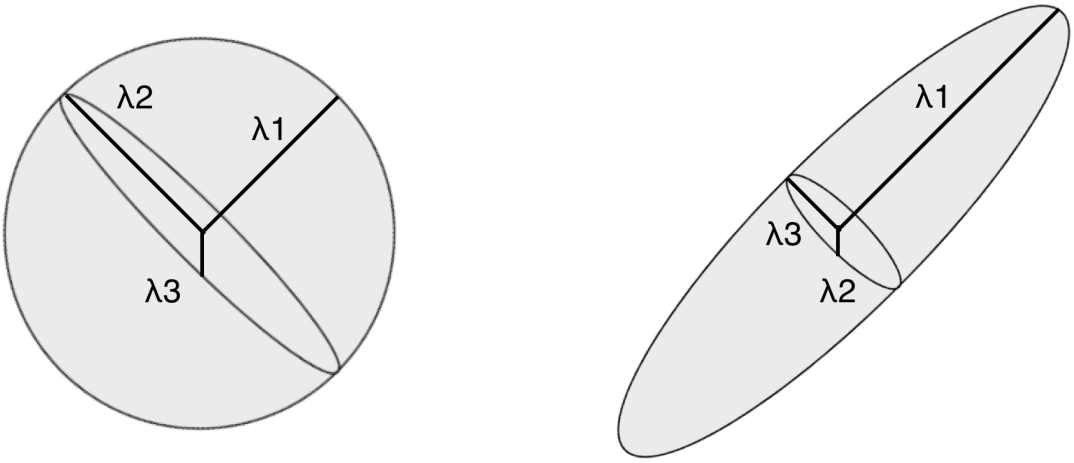

Figure 2.3: Model of typical diffusion tensors. Isotropic diffusion (left) is unrestricted in three directions (sphere). Anisotropic diffusion (right) is restricted in two directions (cigar shape). Image adapted from Diffusion-Imaging.com.

In anisotropic diffusion, we can represent the diffusion in three directions as a tensor. In order to quantify different measures of the tensor, and in turn the tissue of interest, there are several measures worth investigating. The most frequently reported DTI measure is called fractional anisotropy (FA). FA is a measure between zero and one indicating the level of anisotropy in a tensor (Soares *et al.*, 2013). Zero indicating completely isotropic diffusion, with no restrictions in any direction. One indicating completely anisotropic diffusion, with two directions completely restricted.

The mathematical formula for calculating FA is as follows:

$$FA = \frac{\sqrt{3}}{\sqrt{2}} \frac{\sqrt{(\lambda_1 - \lambda)^2 + (\lambda_2 - \lambda)^2 + (\lambda_3 - \lambda)^2}}{\sqrt{\lambda_1^2 + \lambda_2^2 + \lambda_3^2}} \tag{2.7}$$

The above equation involves a weighting of all of the individual eigenvalues from the ellipsoid model (in figure 2.3). In addition to FA, measures of mean diffusivity (MD), axial diffusivity (AD), and radial diffusivity (RD) were also computed. MD is a measure of the average of all three eigenvalues (Soares *et al.*, 2013). The equation is as follows:

$$MD = \frac{\lambda_1 + \lambda_2 + \lambda_3}{3} \tag{2.8}$$

AD is simply a measure of the eigenvalue of the principal (or largest) diffusion direction. In the case of figure 2.3, the principal eigenvalue (for the anisotropic diffusion model) is λ_1, so $AD = \lambda_1$. RD is a measure of diffusion in the outward direction, calculated through averaging the two off principal eigenvalues (Soares *et al.*, 2013). If we were to model RD for the anisotropic model in figure 2.3, it would look as follows:

$$RD = \frac{\lambda_2 + \lambda_3}{2} \tag{2.9}$$

The four measures described above (FA, MD, AD, and RD) will be used in all DTI analysis pipelines described in the following chapters.

2.3 Blood-Oxygen-Level Dependent Imaging

Blood-oxygen-level dependent (BOLD) imaging operates through utilization of the different magnetic susceptibilities of oxygenated and deoxygenated hemoglobin. Oxygenated hemoglobin contains no unpaired electrons, and is weakly diamagnetic. Deoxygenated hemoglobin is created through the release of oxygen, resulting in the exposition of 4 unpaired electrons. These unpaired electrons make deoxygenated hemoglobin strongly paramagnetic. The ratio of concentrations of oxygenated to deoxygenated hemoglobin alters regional T_2 and T_2^*. For example, if the local concentration of deoxygenated hemoglobin were to increase, it would result in a decrease in T_2 and T_2^* effect. If the local concentration of oxygenated hemoglobin were to increase, we would see an increase in the T_2 and T_2^* effect. When a region within the brain is activated, we see in influx of oxygenated hemoglobin in order to adequately perfuse the tissue. This influx of oxygenated hemoglobin leads to an increase in T_2^* effect, and hence, and increase in local signal. The idea is that increased brain activity in a certain cortical region results in increased oxygen demand and an increase in oxygenated hemoglobin locally (along with an increase in signal).

The bulk of analysis with BOLD imaging described in this thesis will focus on functional connectivity. Functional connectivity can be described as the statistical association between two or more anatomically separate regions, based on time-series data collected through multiple BOLD images. Functional connectivity offers information as to the strength, as well as recruitment of connections within the brain. Specifically, our experiment involved the observation of functional connectivity in the resting (wakeful rest) state.

Chapter 3

Literature Review

3.1 Sport-Concussion/Mild Traumatic Brain Injury

Mild traumatic brain injury (mTBI), also commonly referred to as concussion, affects an estimated 1.6 to 3.8 million athletes annually through sport-related head trauma (Langlois *et al.*, 2006). A concussive injury often comes along with a host of post-concussive symptoms, ranging from fatigue, dizziness and headaches, to depression, irritability as well as deficits in memory and executive function (Stern *et al.*, 2011).

In addition to these traditional concussive injuries, athletes participating in contact sports are prone to sub-concussive trauma. Sub-concussive incidents, which have been demonstrated to occur in large numbers throughout an athletes career, often do not present with the common observable signs and symptoms of concussion, and hence, frequently go undetected (Talavage *et al.*, 2014; Gavett *et al.*, 2011). There is evidence which indicates that these repetitive sub-concussive blows place the athlete

at higher risk for developing persistent post-concussive symptoms, structural alterations in the brain as well as neurodegenerative disease such as chronic traumatic encephalopathy (McKee *et al.*, 2009; Tartaglia *et al.*, 2014; Baugh *et al.*, 2012).

In the past decade there has been a steady rise in the number of reported sport-related concussions (Hootman *et al.*, 2007). This increase, however, is most likely a result of heightened efforts in raising awareness of concussion, as well improvement in injury identification and subsequent reporting, rather than a symptom of increased aggression in sports (Hootman *et al.*, 2007; Rosenthal *et al.*, 2014). As one may expect, the sports which consistently report the highest concussion exposure rates include high intensity, contact focused sports such as American football and ice hockey (Marar *et al.*, 2012). However, in lieu of the considerable and rapidly expanding body of concussion research, many professional sports organizations refuse to acknowledge a potential connection between repeated sports-related brain trauma and long-term brain health. This seemingly antiquated stance could be attributed to the lack of a robust method for measuring long-term neurodegenerative effects of repetitive concussive injuries.

Traditional CT and MRI clinical imaging techniques frequently struggle to identify changes in the brain after mild concussive injury, as most are focused on identifying structural alterations and lack the sensitivity to observe microstructural alterations (Belanger *et al.*, 2007; Shenton *et al.*, 2012; Bigler, 2004). There have been further developments in recent years with the inclusion of DTI and BOLD functional MRI into study protocols, both of which have demonstrated increased sensitivity to minute changes common to mild traumatic brain injuries.

The following subsections will focus on detailing recent findings in the literature

which involve DTI, BOLD fMRI, and advanced cortical measuring methods. To date, the literature involving sport-related concussion has been somewhat sparse. There have been even fewer studies examining the effects of sport-related concussion on a long term basis, $\geq$ 10 years since retiring from play. The focus of this literature review will remain on findings in populations of retired athletes. This is due to inconsistencies in findings within the literature of sport-concussion in current athletes, versus that observed on a long term basis in retired athletes. Further sections detailing results of neuroimaging and neuropsychological testing will delve further into these inconsistencies.

3.1.1 Diffusion Tensor Imaging

White matter integrity, measured through DTI, has been previously demonstrated to a be a key indicator of patient outcome immediately after a mTBI/TBI. There have been fewer studies investigating the effectiveness of DTI in evaluating long-term outcome with a history of sport-related concussion. However, the hope is that DTI is able to highlight differences in microstructural integrity which may be present, and offer some insight into interpretation of the results. DTI metrics such as those described in the previous chapter (FA, MD, AD, and RD), offer an indirect measure of white matter tissue integrity, through the estimation of a diffusion tensor for each voxel in the brain. Traditionally, studies investigating the effects of mTBI/TBI or sport-related concussion occur in the acute or semi-acute phase. These follow hours to weeks post-injury. In this work, however, we aim to quantify effects of a lifetime of exposure to sport-related concussion, by examining former athletes many years after retiring from play (and suffering their most recent concussion).

Although it is difficult to directly attribute diffusion tensor measures to underlying white matter tissue, ex vivo studies, along with a growing body of mTBI research, has offered insight into common findings post-injury. In general, white matter tracts damaged in a concussive injury will exhibit increased measures of FA, and decreased measures of RD in the acute phase (hours to days post-injury) (Wilde *et al.*, 2008). This is thought to be due to effects of cytotoxic edema (energy crisis, cells draw in water), and inflammation (Wilde *et al.*, 2008). As the subject progresses into the sub-acute phase (days to weeks), decreased measures of FA, along with increased MD or RD are commonly exhibited (Shenton *et al.*, 2012). This is thought to reflect myelin or axonal damage, or reduced axonal packing density or coherence (Shenton *et al.*, 2012). Little is known about the long-term, or chronic effects of a history of concussion. To date, there have been very few DTI studies examining athletes of a high impact sport, many years after retiring from play. Studies involving DTI analyses techniques with former athlete populations are described below.

Recently, Multani *et al.* investigated a population of 18 former professional athletes of the CFL (age 49.6 ± 12) through imaging and neuropsychological testing (Multani *et al.*, 2016). The average time since retirement from professional play was 16.2 ± 13 years, with average CFL career length equal to 7.8 ± 4. This subject group is very similar to our recruited CFL subjects, in terms of both mean age, time since retirement, and career length. In addition, Multani *et al.* used the same voxel-based statistical analysis package (TBSS) as was used within this study. They reported significantly increased measures of AD in the retired CFL population when compared to a group of healthy controls (along with a greater number of symptoms in behavioural categories including, memory, executive function, language, behavioural changes, and

headaches). Regions of increased AD were localized to the right superior longitudinal fasciculus, corticospinal tract, and anterior thalamic radiations. As previously described in the introductory chapters, the superior longitudinal fasciculus is an association tract (connecting different cortical regions within the same hemisphere), involved with visual memory. The corticospinal tract and anterior thalamic radiation are projection tracts (connecting cortical regions with subcortical structures), and are involved with voluntary movement and memory formation, and executive function, respectively. Increased AD found within the athlete population was attributed to subtle changes which axons may experience after a sports-related concussive injury. Due to the repetitive nature of many of these sport-related injuries, small axonal changes may eventually lead to disruption in transport, swelling, and axonal detachment over time (Multani *et al.*, 2016). There is also evidence which indicates that this axonal degeneration progresses over the years, and may be the underlying cause of the altered AD measures observed in this sample population (Multani *et al.*, 2016).

Another study by Goswami *et al.* involved cognition testing, along with MRI on a population of 19 former professional athletes of the CFL (age 50 ± 12), compared to an age and sex matched group of 17 control subjects. The player range varied from $34 - 74$ years, with the time since retirement varying as well. It was found that AD measures within the uncinate fasciculus correlated negatively with error rates, and aggression scores in behavioural testing (Goswami *et al.*, 2016). However, their DTI analysis was restricted to the uncinate fasciculus. The group found no significant regions of difference through DTI metrics between retired athletes and controls in other regions.

In a study by Sasaki *et al.*, the effects of a history of clinically symptomatic

concussion in athletes was investigated through neuroimaging and behavioural testing (Sasaki *et al.*, 2014). In the study, 16 Canadian Inter-university Sports ice hockey athletes with a history of concussion (age 21.7 ± 1.5) were compared to a group of 18 athletes without a history of concussion (age 21.3 ± 1.8). The athletes underwent scanning at the end of a season of a Canadian Inter-university Sports ice hockey. Unfortunately, the time line since retiring from play does not match up with that of our recruited subjects, but both are classified as the chronic phase of injury. TBSS analysis between those with a history of concussion, and the healthy controls revealed many differences in DTI metrics. A significant increase in FA and AD and a significant decrease in RD was noted in several regions in the concussed group, compared to the controls. Regions of difference in FA and RD included, the right posterior limb of the internal capsule, the right corona radiata, and the right temporal lobe. Increased measures of AD within subjects with a history of concussion was recorded within the left corona radiata (Sasaki *et al.*, 2014). Interestingly, the authors found no correlation of DTI measures with the results of the computerized immediate post concussion assessment and cognitive test (ImPACT), or the sport concussion assessment tool 2 (SCAT2) symptomatology scoring. The authors suggested increased measures of FA, and decreased measures of RD, may be attributed to neuroplastic processes within the brain following repetitive injury (Sasaki *et al.*, 2014).

Work done by Hart *et al.* investigated the effects of a history of sport-related concussions in a population of retired NFL athletes. In total, 26 retired players (mean age 61.8) underwent neuroimaging analyses, alongside 26 age and sex matched controls. Of the 26 athletes, 14 were identified as symptomatic (impairments of cognition or mood). These 14 athletes were compared to a subset of 14 healthy

controls through DTI analysis. It was found that symptomatic controls exhibited diffuse reductions in measures of FA bilaterally in the frontal and parietal regions, along with the corpus callosum and left temporal lobe. No differences in measures of FA were noted between the remaining 12 asymptomatic athletes, and controls. This study only focused on measures of FA, although including analysis of MD, AD, and RD could have added significant value. The authors concluded with the observation that cognitive deficits and depression appear more common in aging retired NFL players than the normal population, with differences correlating with changes in white matter integrity (Hart *et al.*, 2013).

3.1.2 Functional MRI

Resting state fMRI, and subsequent analysis of the default mode network (DMN), provides insight into relationships between brain regions, without the need to perform a cognitive task. Analysis of these low frequency fluctuations in the resting temporal BOLD signal can offer a window into understanding patterns of intrinsic connectivity within anatomically separate regions of the brain (McDonald *et al.*, 2012). The DMN is comprised of three key regions, the posterior cingulate cortex, medial prefrontal cortex, and angular gyri. Generally, resting state fMRI measured in an acute to semi-acute phase post-concussion include interruptions to the DMN, often presenting as decreases in connectivity within frontal regions (McDonald *et al.*, 2012). To date, there have been several studies examining former professional athletes through functional connectivity mapping. However, these studies often reach different conclusions in terms of regions of interrupted connectivity. This, in part could be attributed to the inhomogeneity of concussion, where each subjects specific anatomy may result

in different transfer of forces through the brain. Relevant studies in retired athletes follow below.

Hampshire *et al.* investigated a population of retired athletes of the NFL using fMRI methods, along with structural MRI (Hampshire *et al.*, 2013). A total of 13 former NFL players were recruited, with a mean age of 54 years, along with a group of 20 aged matched healthy controls. The authors found that during a resting-state fMRI task, NFL alumni exhibited lowered measures of functional connectivity within the dorsal frontoparietal network, relative to controls. More specifically, connectivity was decreased between the parietal cortex, dorsolateral prefrontal cortex, and the frontopolar cortex. This, suggesting that retired NFL athletes have deficits in connectivity within the dorsal planning network, (including portions of the default-mode network) involved in thoughts of others, memories of the past, and planning in the future.

A study by Ford *et al.* investigated the long-term effects of multiple sport-related concussions on event-related memory tasks in fMRI (Ford *et al.*, 2013). A population of 27 former professional NFL players (who have played a minimum of 2 seasons of professional play, age 63.4 ± 5.9) were compared to a group of 14 healthy, age, sex, and education-matched controls (age 62.2 ± 6.3). The authors found no significant differences in terms of behavioural memory tasks between the low (0, 1, 2) and high (3 or more) concussion groups. This lack of difference could be attributed to the lack of knowledge of concussion, and injury reporting. However, the two groups of players (low and high concussion) exhibited different activation patterns in fMRI during memory retrieval exercises. These differences could suggest potential functional inefficiencies in those who have suffered multiple concussions. The study also reported a

link between the number of previous concussions and functional activity within the medial temporal lobe and inferior parietal lobe (Ford *et al.*, 2013). Overall, Ford *et al.* describe their findings as supporting the hypothesis that a history of repeated sport-related concussions could result in alterations to underlying functional connectivity patterns.

The study by Goswami *et al.* described in the section above, involved a robust neuroimaging investigation of a population of 19 retired athletes of the CFL, compared to healthy controls. In addition to the changes found in measures of DTI, the authors also probed measures of functional connectivity through fMRI. It was found that retired CFL athletes presented with elevated functional connectivity within the anterior temporal lobe and the orbitofrontal cortex, which could be associated with the increased impulsivity that retired athletes demonstrated.

3.1.3 Cortical Thickness

The work done by Goswami *et al.* described in the previous section also involved measurement of cortical thickness, through the use of a similar pipeline to that presented in this thesis. It was found that when compared to healthy (age and sex matched) controls, the retired CFL population ($n = 19$, age 50 ± 12) demonstrated significant cortical thinning within the left anterior temporal lobe (Goswami *et al.*, 2016).

A study by Koerte *et al.* involving 15 former professional German soccer players (age 49.3 ± 5.1) investigated the effects of years of heading the soccer ball through the use of several neuropsychological tests, along with cortical thickness measures (Kontos *et al.*, 2012). The authors found that soccer players faired worse than controls on delayed memory tasks, but were otherwise normal for neuropsychological testing. As

for cortical thickness measures, soccer players exhibited significantly decreased measures with age, compared to controls. Specific regions of decreased cortical thickness included the right hemisphere parietal, and occipital lobes (this also correlated with lifetime heading estimates) (Koerte *et al.*, 2016).

Casson *et al.* investigated a population of 45 retired athletes of the National Football League (NFL) (age 45.6 ± 8.9). The range of athlete age was from $30 - 60$, with some athletes recently retiring, and others exceeding 10 years post retirement from sport. It was found that 2 retired NFL athletes exhibited abnormally enlarged ventricles and thin corpus callosum, 34 athletes had a cavum septum pellucidum (with 3 exhibiting abnormally large cavum septum pellucidum). cavum septum pellucidum is one of the distinguishing features of individuals who present postmortem with the progressive, neurodegenerative disease, chronic traumatic encephalopathy (CTE) (McKee *et al.*, 2009). Unfortunately, the authors did not perform higher-level group-based analysis on the data, which would help in providing a comparable basis with findings of other neuroimaging studies.

Tremblay *et al.* investigated the effects of participation in university level sports (ice hockey and football) in a population of 15 subjects with a history of sport related concussion (age 60.87 ± 7.51). It was demonstrated that retired athletes showed reduced verbal fluency, and altered episodic memory on delayed recall and recognition (Tremblay *et al.*, 2012). As for the results of structural imaging, the subject population with a history of sport-related concussions demonstrated exacerbated cortical thinning, when compared to the thinning observed in regular aging. These diffuse decreases in cortical thickness correlated with decreases detected in episodic memory within the formerly concussed athlete group (Tremblay *et al.*, 2012). However, there

were no grey matter anomalies observed between the former concussed athletes and healthy athletes when comparing between groups with similar age. In addition to accelerated cortical thinning due to aging, there were also abnormal enlargements of the lateral ventricles, another finding in deceased athletes with verified CTE (Tremblay *et al.*, 2012; McKee *et al.*, 2009).

Chapter 4

Problem Definition and Hypothesis

4.1 Problem Definition

As detailed in the previous section, sport-related concussions are occurring in extreme numbers, with upwards of 3.8 million concussions recorded annually in the US (Langlois *et al.*, 2006). In this section we will further describe the potential consequences of this rapidly expanding health crisis.

For almost a century, we have had knowledge of the association between sport-related head trauma and poor later life outcome. However, there has been little regard for long term athlete outcome. In 1928 Martland detailed a degenerative condition in boxers, referred to as "punch drunk". So named due to similar symptoms to that of an intoxicated person, brought on a result of repeated blows to the head. However, it was not until recently that these conditions were observed in populations of athletes in other sports. Omalu *et al.* was the first to report symptoms of chronic traumatic encephalopathy (CTE), a neurodegenerative disease thought to be caused by repetitive brain trauma, in the autopsy of a retired professional football athlete

of the National Football League (Omalu *et al.*, 2005). Since that discovery, 110 of 111 investigated brains of deceased former NFL players have exhibited signs of CTE (Boston University CTE Center).

CTE is characterized through the accumulation of hyperphosphorylated tau protein, and TDP-43, presenting with cognitive (memory impairment, and executive dysfunction), mood (depression, irritability, and suicidality) and behavioural impairments (impulse control, substance abuse, and aggression)(McKee *et al.*, 2009; Baugh *et al.*, 2012). Specific anatomical changes present in autopsy include, atrophy of the brain and reduced brain weight, in addition to atrophy of the frontal and temporal cortices along with the medial temporal lobe (McKee *et al.*, 2009). There is also general thinning of the corpus callosum, and atrophy of white matter tissue in cerebral subcortical regions. Anterior cavum septum pellucidum (when the septum pellucidum space is filled with cerebro-spinal fluid), in addition to dilation of lateral and third ventricles is also common (McKee *et al.*, 2009). There is currently no neuropathologically validated clinical diagnostic criteria for CTE, however, recent advances in neuroimaging present an opportunity for identifying a biomarker to disease progression.

4.2 Proposed Solution/Aim of Work

Taking a step away from CTE, there still remains a large gap in knowledge of concussive injury progression between the acute range (hours to days), and the chronic phase (weeks to years) post injury. In this thesis, we sought to identify changes present in a population of retired athletes of the Canadian Football League (CFL) with a history of sport-related concussion, through utilizing advanced neuroimaging methods.

Thus far, there have been very few studies involving retired professional athletes focused on investigating long term effects of sport-related concussion. And to date, not a single study has combined neuroimaging modalities (DTI, rs-fMRI, and cortical thickness measures) with electroencephalogram (EEG) analysis paradigms, and neuropsychological testing. Hence, our study truly offers the potential for novel insight into the long term consequences of sport related-concussion.

4.2.1 Objectives

The focus of this research was to develop a pipeline for the neurological assessment of retired athletes of the CFL, through the inclusion of multiple modalities. The ultimate goal being to further knowledge of the potential long term consequences of participating in high impact sports. Through providing detailed insight into neurological findings as measured through MRI, along with evidence of progressive age related decline, the ultimate goal was to suggest a potential biomarker for clinical projection of an athletes long term neuropathological outcome. These objectives were to be investigated through the following techniques:

- Investigation of microstructural integrity as measured through advanced DTI analyses. Comparing the retired CFL population to a group of age and sex matched concussion free controls through a z-scoring methodology.

- Probing of functional connectivity patterns in the resting state, measured through seed based fMRI analyses. Again, comparing the two populations through cluster-wise z-scoring analysis.

- Examination of cortical integrity through measuring whole brain cortical structure. Measures between groups being compared through z-scoring methods.
- Perform a multitude of neuropsychological assessments in order to evaluate individual effectiveness by correlating with imaging results.
- Perform analyses within the retired CFL population, based on number of years played professionally, primary position played, and athlete age.

4.2.2 Hypothesis

It has been demonstrated that the use of DTI, fMRI and cortical thickness measures are useful techniques in evaluating the brain's functional and structural integrity after concussion or mTBI. In this work, we hypothesize that these techniques can be utilized to effectively measure alterations in neuropathology in a group of former athletes of the CFL with a history of sport-related concussion. Based on results of previous work discussed in the literature review, we hypothesize the following:

- A reduction of measures of FA, along with an increase in AD, and potentially MD will be observed in white matter tracts which are commonly damaged in concussion. These including, the corpus callosum, corona radiata, and longitudinal fasciculi.
- Alterations to functional connectivity within the DMN. Specifically, decreases in connectivity in regions associated with white matter alterations.
- Cortical thinning in regions common to injury, such as the frontal or temporal lobes.

- Strong correlation of neuropsychological testing measures with outcomes of imaging metrics, confirming the effectiveness of clinical techniques.
- Increased neuroimaging abnormalities due to increased position related sports-contact and years of play in the CFL.
- Accelerated age-related changes in the retired athletes as measured through neuroimaging abnormalities.

Chapter 5

Materials and Methods

This section will provide an overview of the materials and methods utilized within the performed analysis detailed in this thesis.

5.1 Study Overview/Demographics

Former athletes of the CFL, having partaken in at least 3 seasons of professional play, were recruited from regions surrounding Hamilton, Niagara and Toronto for testing. The goal was to run the retired CFL population through detailed MRI, EEG, and neuropsychological testing protocols, on a single occasion. In total, 23 former athletes were recruited for the study. However, due to issues with imaging data and patient cooperation in the magnet, there were 4 exclusions made on the MRI side, leaving 20 remaining datasets for cortical thickness measures and 19 for DTI and fMRI methods. On the EEG side, only a single exclusion was made, leaving 22 total subject datasets. The average age of the participants was 58.1 years ($n = 19, 58.1 \pm 6.5$). Of these participants, all 19 were male. This thesis focuses on the imaging and

neuropsychological aspects of the testing.

All recruited subjects received an MRI, EEG, and neuropsychiatric testing. The Immediate Post-Concussion Assessment and Cognitive Testing (ImPACT), Beck Depression Inventory II (BDI-II), Short Form Health Survey (SF-36), and Post-Concussion Symptom Scale (PCSS) served as the basis for comprehensive neuropsychiatric evaluation. The ImPACT test gives an assessment of memory and reaction time. The BDI-II, SF-36 and PCSS examined overall mental and physical well being.

On the neuroimaging side, the detailed (hour long) MRI scan protocol consisted of a high resolution T1 weighted structural scan, a diffusion weighted scan, and a functional BOLD scan. These three scan techniques are robust in their ability to detect different neuropathology, and offer information as to the structural, micro-structural, and functional aspects of the brain. EEG testing included the measurement of event related potentials. Event related potentials are useful in evaluating different aspects of cognition, and cognitive function.

In addition to the former athlete population, a subset of 20 age and sex matched controls were recruited from the Hamilton area for EEG, and neuropsychological testing. However, these subjects were not brought in for the MRI scan protocol due to funding constraints.

Controls for use in MRI analysis procedures were sourced from online data repositories. Anatomical, functional and diffusion data to serve as healthy control subjects for group comparison were downloaded from the 1000 Functional Connectomes Project, specifically the Milwaukee dataset (fCONN), and Alzheimers Disease Neuroimaging Initiative (ADNI) databases (Mennes *et al.*, 2013; Jack *et al.*, 2008). A group of healthy controls ($n = 19, 52.0 \pm 4.7$) from the fCONN database served as the

basis of comparison for probing group differences in measures of functional activity. fCONN focuses on the development of a probabilistic reference system for the human brain, through acquisition of a large amount of patient data spanning across a wide age range (Mennes *et al.*, 2013). A group of healthy controls ($n = 25, 63.1 \pm 2.5$) from the ADNI database was used for analysis of group differences in diffusion measures. A slightly larger group from the same database ($n = 29, 63.8 \pm 2.8$) was used for cortical thickness measures (Jack *et al.*, 2008).

Table 5.1: Athlete Data Statistics. Groupings based on age, years of play (YOP) professionally and frequent or less frequent contact groupings are indicated.

(Years)	*Subjects*	*CFL Career*	*Age* ≤ 58	*Age* > 58	*YOP* ≤ 10	*YOP* > 10	*Freq Cont*	*Less Freq Cont*
Number	20	-	9	11	11	9	13	7
Mean	58.1	8.1	52.2	62.7	57.7	58.3	58.2	57.6
SD	6.5	3.8	4.9	2.2	5.6	7.22	5.6	7.6
Minimum	45	3	45	59	48	45	46	45
Maximum	66	14	58	66	66	66	66	66

Table 5.1 details all relevant measures of the recruited former athlete population. This includes information of average age, and average length of professional careers. Sub-groupings within the retired athlete population were derived based on professional career length and position played. Professional career length groups were chosen according to a cutoff length of 10 years (≤ 10 vs > 10 years of play). Position based groups were decided based on whether the position involved frequent contact:

center, running back, full back, guard and tackle, defensive tackle, linebacker and defensive end, or less frequent contact: quarterback, wide receiver and tight end, safety and cornerback.

Table 5.2 includes relevant measures for the control datasets. Age and number of subjects are included, along with origin of subject data.

Table 5.2: Control Data Statistics.

(Years)	*fCONN (fMRI)*	*ADNI (Anat)*	*ADNI (DTI)*
Number	19	29	26
Mean	52.0	63.8	63.1
SD	4.7	2.8	2.5
Minimum	44	60	59
Maximum	58	66	67

5.2 MRI Scan Protocol

Recruited subjects were scanned using a General Electric MR750 Discovery 3T MRI scanner with a 32-channel RF receiver coil (General Electric Healthcare, Milwaukee, WI). Following a routine 3-plane localizer and calibration scan for parallel imaging, a 3D inversion recovery-prepped T1-weighted anatomical data set was acquired (fSPGR, axial acquisition, TE/TR/flip angle = 4.25/11.36/12°, 256x256 matrix with 1mm slice thickness with 25.6cm FOV, 1mm isotropic acquisition). To assess functional connectivity, resting state functional BOLD data was collected using an echo

planar imaging (EPI) sequence with FOV = 22cm, image matrix = 64x64; flip angle = 90°; echo time (TE) = 35ms; repetition time (TR) = 2000ms; slice thickness of 3mm; and 175 temporal points. Axial Diffusion Tensor Imaging (DTI) data was acquired using a dual echo EPI sequence with 60 non-coplanar directions, TE/TR = 87/8800 ms, b = 1000 s/mm^2, 122 x122 matrix, 70 slices, 2.0 mm slice thickness, 244 mm FOV, ASSET = 2.

Anatomical, functional and diffusion data parameters from the 1000 functional Connectome Project (fCONN) and Alzheimer's Disease in Neuroimaging (ADNI) databases, respectively, are as follows. All control subjects had no history of neurological or psychiatric disorders. For the fCONN dataset, resting-state conditions included subjects refraining from any movement or excess mental activity as well as keeping their eyes closed during the scan. Scans were recorded on a 3T GE scanner, using an EPI sequence along with the following scan parameters: 23 contiguous axial slices; 4 mm slice thickness; 64 x 64 mm matrix with a 4 x 4 mm ^{2} in-plane resolution; TR/TE = 2000/50 ms; flip angle 90°; and 128 temporal points). A group of healthy subjects to serve as controls in the cortical thickness measures (N=29 63 $\pm$ 1.9yo) and for use in the diffusion MRI analysis (N=25 (63 $\pm$ 2.4yo) were downloaded from the ADNI database. The anatomical and diffusion data was acquired at 14 different sites across North America using 3T GE Medical System scanners. Anatomical spoiled gradient echo (SPGR) acquisition parameters are as follows: 256 x 256 matrix; voxel size = 1.2 x 1.0 x 1.0 mm^3; TI = 400 ms; TR/TE = 6.98/2.85 ms; flip angle = 11°. Diffusion weighted imaging data was recorded on the same 3T GE magnet magnet with the following parameters: 256 x 256 matrix; voxel size 2.7 x 2.7 x 2.7 mm^3; TR = 9000 ms and 46 separate volumes (5 T2-weighted B0 volumes; and 41

diffusion-weighted images with b = 1000 s/mm^2).

5.3 Processing Pipeline

Following acquisition of study data, the next step was to design an analysis procedure in order to extract meaningful information from the data. The following sections describe, in detail, the procedures implemented. Due to the similarity of scan parameters between the protocol for recruited former athletes, and the image data sourced online, there should be minimal differences due to different scan sites. All described procedures were applied in the same manner to both imaging subject datasets.

5.3.1 Cortical Thickness Measures

In order to allow for more involved analyses to be implemented, all T1-structural images were first brain extracted using the Brain Extraction Tool (BET2) in FSL (Jenkinson *et al.*, 2005). BET2 removes non-brain tissue from whole brain structural MR scans through a robust thresholding and registration procedure. Skull-stripped images then became input to a second level analysis, aimed at detailing cortical structures. An overview of the cortical thickness procedure is outlined in figure 5.1.

Segmentation, reconstruction and measurement of brain structures across retired athlete and control data was performed through the use of the FreeSurfer toolkit (version 6.0.0), and the implementation of SHARCNET high-performance computing clusters (Misc, 2017). Results of each stage of the cortical thickness segmentation procedure can be viewed in figure 5.2.

In order to ensure proper structure segmentation, manual quality control was

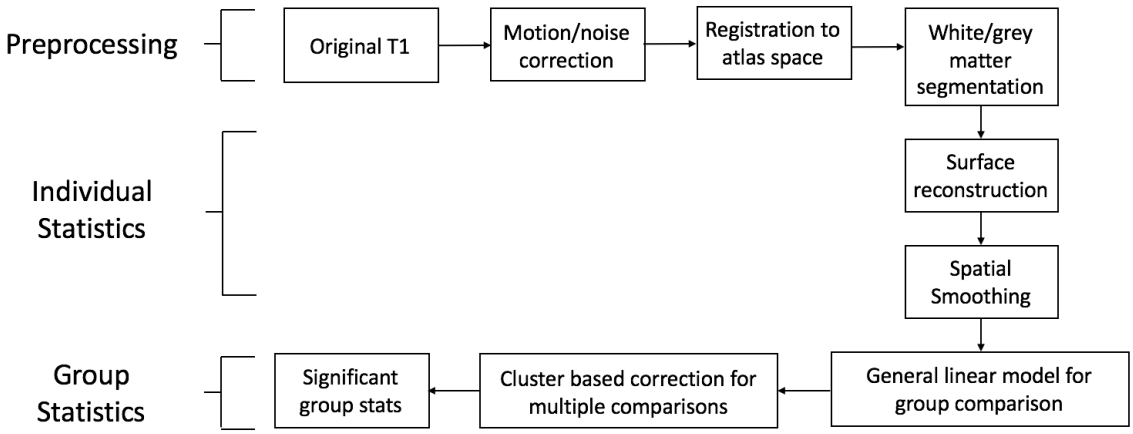

Figure 5.1: An overview of the cortical thickness analysis pipeline.

performed through inspection of individual segmented image data. Voxel-wise cortical thickness maps were generated through the use of group (rCFL vs controls) as a factor, and subject age as a covariate.

Cluster-wise correction for multiple comparisons was performed through the creation, smoothing and thresholding of a z-score map (with a 5mm full width half maximum kernel). Regions of maximum cluster intensity in the output z-maps were then noted. In order to correct for multiple comparisons, the above procedure was repeated for 5000 iterations using the false discovery rate, $p < 0.05$. The resulting images were cluster-corrected images, comparing measures of cortical thickness in the left and right hemispheres between rCFL and control groups.

The same cluster-wise correction for multiple comparisons procedure described above was used in the individual data comparisons as well as for the within rCFL group comparisons.

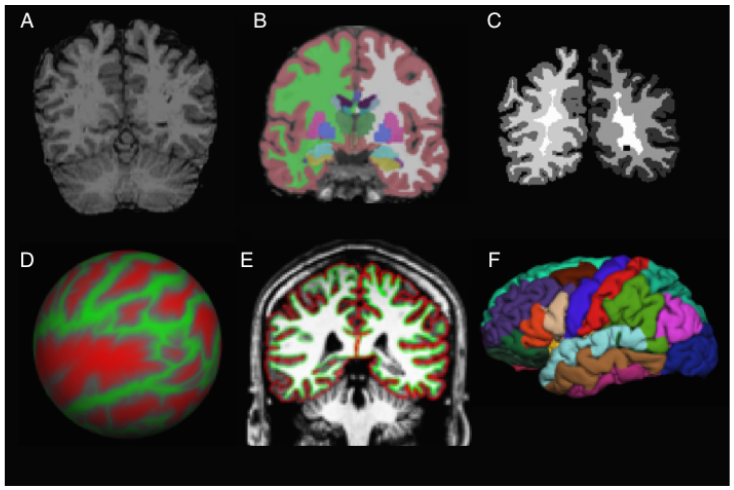

Figure 5.2: Visual depiction of the segmentation process of the FreeSurfer toolkit during cortical thickness analysis. Image (A) depicts the skull-stripped T1 weighted image. (B) shows the volumetric labeling surface, and (C) visualizes the segmented white and grey matter structures with the brain stem and cerebellum removed. (D) shows the surface atlas registration (unwrapped target). (E), and (F) show the surface extraction and gyral labeling, respectively.

5.3.2 Diffusion Tensor Imaging

Before performing more in depth analysis, the diffusion weighted scans were skull-stripped, corrected for eddy-current induced distortions, and head motion. These processes were implemented through the use of the FSL BET2, FSL eddy, and FSL FLIRT tools (Jenkinson *et al.*, 2005; Andersson and Sotiropoulos, 2016). The overall DTI analysis procedure is outlined in figure 5.3.

A whole-brain, voxelwise, connectivity based parcellation analysis of all DTI data was completed through the use of FSL Diffusion Toolbox (FDT) and Tract-Based Spatial Statistics (TBSS) programs (Johansen-Berg *et al.*, 2004; Smith *et al.*, 2006). Through FDT, diffusion tensors were reconstructed by the estimation, and fitting of a tensor model to the raw diffusion data. This tensor fitting resulted in images of FA, MD, AD, and RD. AD is a measure of the principal diffusion eigenvector (AD =

λ_1). RD is a measure of the average of the second and third tensor eigenvectors (RD $= (\lambda_2 + \lambda_3)/2$).

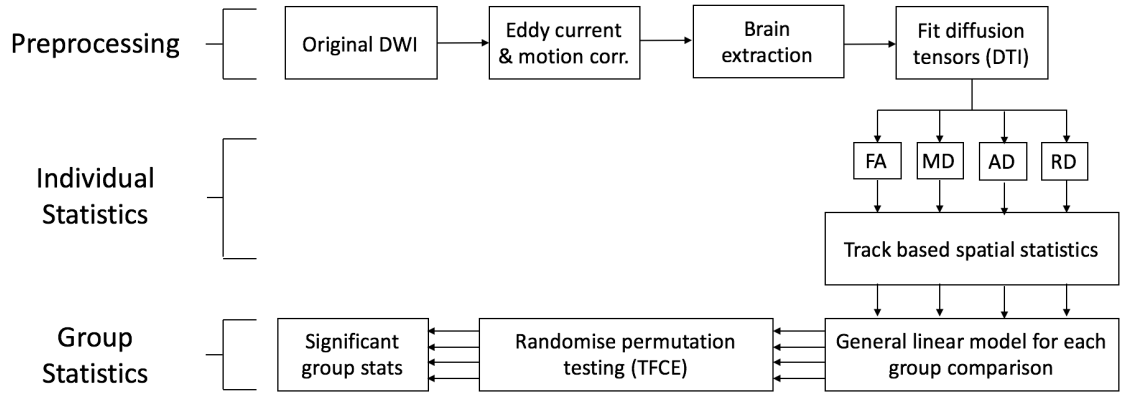

Figure 5.3: Visual description of the overall DTI analysis pipeline.

After completing the tensor fitting procedure, the next step was to create the baseline data necessary for further high level statistical analysis in order to allow for probing of group differences. Through TBSS, a common registration target for all subject data was created via non-linear transformation matrices and an affine transform. Each subjects aligned DTI tensor measures (FA, MD, AD, and RD) were projected onto a tract-invariant skeleton target. This target was created from all of the individual datasets, and hence, is representative of all included subjects white matter anatomy. In order to preserve white matter tissue, and remove non-desirable brain structures (grey matter and CSF), the skeleton was carefully thresholded and manually edited. The final skeletons (one for each DTI metric) represent most consistent white matter pathways across all subjects. A skeleton of FA, along with images from each of the processing steps followed to create it can be seen in figure 5.4.

Voxel-wise statistics identifying differences between different populations (retired athlete vs controls) were then performed on the created skeletons. In addition to

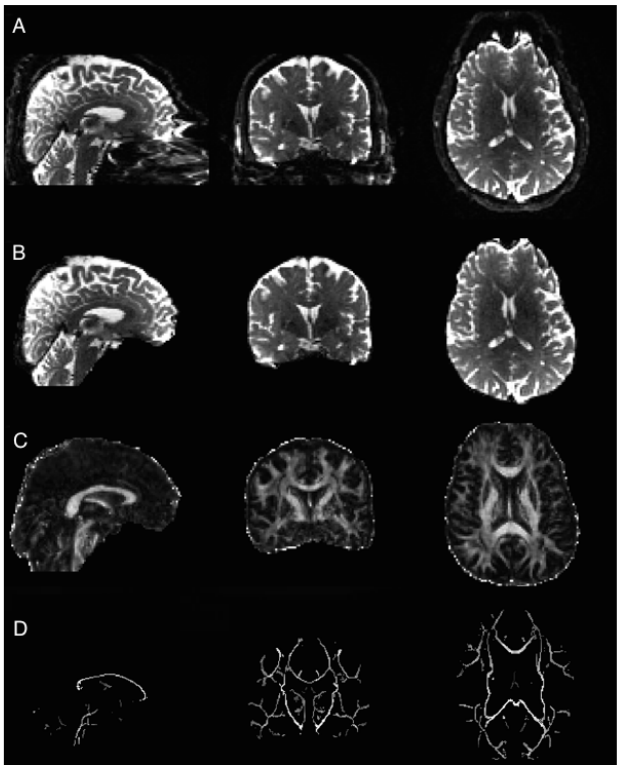

Figure 5.4: Visual depiction of the resulting output from each step of the processing pipeline during DTI analysis. Image (A) shows the original DW image, while (B) shows the brain extracted DW image. Image (C) visualizes the FA image which was created through tensor fitting. Image (D) is of the FA tract-invariant skeleton used for further statistical analysis.

the voxel-wise analysis, cluster-based identification of significant regions of interest (ROI) based on the ICBM-DTI-81 white matter labels atlas was also performed. The ICBM-DTI-81 white matter atlas includes 48 individual white matter tracts, identified through averaging diffusion MR maps from 81 subjects ($n = 81$, $mean = 39$, $range = 18 - 59$) (Mori *et al.*, 2005). The atlas is shown in figure 5.5.

Group differences in DTI measures were probed through permutation testing methods, via the use of the FSL Randomise program (Winkler *et al.*, 2014). A linear model placing patients and controls in different subcategories and including

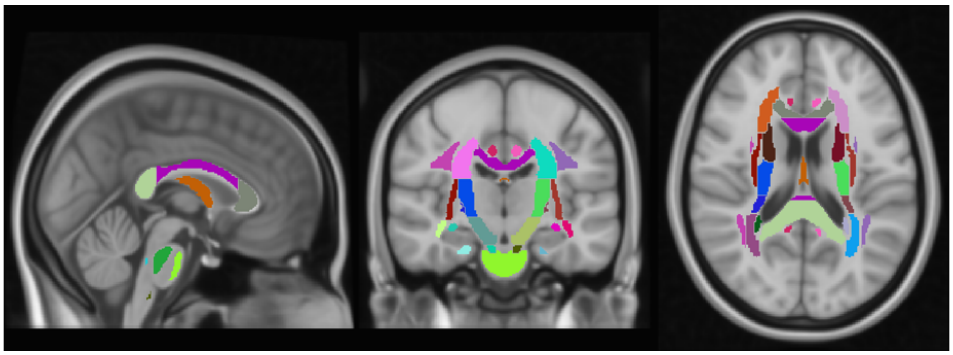

Figure 5.5: ICBM-DTI-81 white-matter labels, with 48 white matter structures included, viewed on top of a standard MNI T1 1mm atlas.

subject age as a covariate in the analysis, provided the basis for comparison. In the following sections within this chapter, more description into the generation of these linear models for each individual comparison will be given.

Subsequent application of Threshold-Free Cluster Enhancement (TFCE) using the designed linear model, provided the basis for observing and quantifying any significant group differences in structural integrity between subject populations. Further statistics were performed individually, and between groupings based on years of professional play, as well as position and athlete age as noted previously in table 5.1.

5.3.3 Blood-oxygen-level-dependent Imaging

As detailed previously in the cortical thickness section, T1-structural images (used simply for registration of the rs-fMRI datasets) were brain extracted using the Brain Extraction Tool (BET2) in FSL (Jenkinson *et al.*, 2005). BOLD rs-fMRI data was then motion corrected using the MCFLIRT tool included in FSL (Jenkinson *et al.*, 2002).

To perform seed based ROI analysis on rs-fMRI data, one first needs to decide

on a location for seeding, then create the seeds. Randomly selecting seed locations within the brain will not reveal much useful information. Having prior knowledge of the location of networks of interest is necessary in order to properly place seeds. As described in the introduction, the DMN was selected as a robust network for seed based analysis.

The overall analysis pipeline followed the procedure detailed by Uddin *et al.*, with slight modifications to the masking and statistical methods (Haneef *et al.*, 2014; Uddin *et al.*, 2009). Figure 5.6 offers an overview of the analysis pipeline.

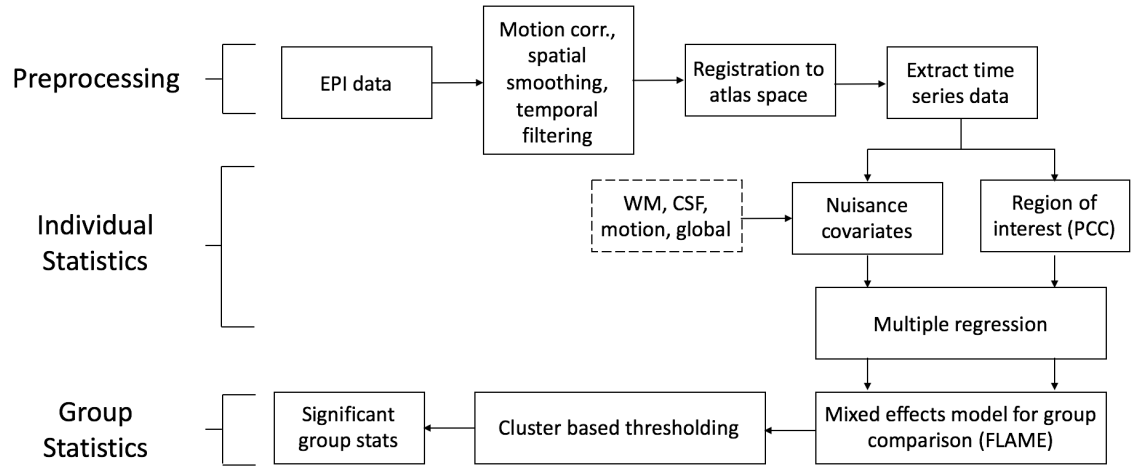

Figure 5.6: Visual description of the overall fMRI analysis pipeline.

A region of interest within the core of the DMN, in the posterior cingulate cortex, was created on a standard 1mm MNI atlas through placement of a 6mm square. The posterior cingulate cortex ROI was centered at MNI coordinates $(x, y, z = 2, -60, 36)$, similar to the location described in prior studies (Uddin *et al.*, 2009). This selected ROI coordinate location is visualized in figure 5.7.

Cerebral spinal fluid and white matter regions are not commonly included in analysis of BOLD data. In order to remove the contributive effects of these regions,

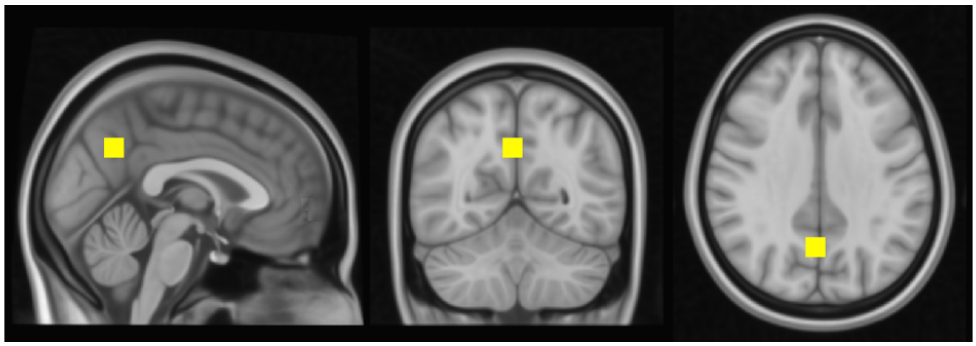

Figure 5.7: Placement of the posterior cingulate cortex ROI, viewed on top of a standard MNI T1 1mm template.

personalized brain masks were created for each subject's anatomical data through FMRIB's Automated Segmentation Tool (FAST) (Zhang *et al.*, 2001). Next, FMRIB's FEAT analysis package was used to filter and spatially smooth the functional datasets (with a 5mm full-width-half-maximum). FEAT also works to register the subjects' functional dataset to their anatomical dataset using a Boundary-Based Registration (BBR) algorithm. This intermediate registration step is followed by a final registration to a standard Montreal Neurological Institute (MNI) 152 1mm atlas image (Jenkinson *et al.*, 2012).

The output transformation matrices for each subject (created through the anatomical to standard space transform) were used to fit the previously created cerebrospinal fluid (CSF) and white matter (WM) masks to the patients individual atlas data. Time series data was then extracted from the standard space functional data through the CSF and WM masks, and normalized through using R (R Core Team, 2013). A similar process was used for implementation of the posterior cingulate cortex ROI. Time series data was extracted and normalized, and used within a GLM as regressors in a partial correlation analysis.

Normalized times series of CSF and WM were included as nuisance covariates,

and the posterior cingulate cortex data was used for correlation within a higher level regression analysis in FEAT through a General Linear Model (GLM). Group statistics were carried out using FMRIB's Local Analysis of Mixed Effects (FLAME). FLAME uses complex methods in order to model and estimate the random-effects component of measured inter-session mixed-effects variance. FLAME offers an accurate estimation of the true degrees of freedom, and the true random-effects variance at each voxel (Jenkinson *et al.*, 2012). FLAME resulted in voxel-wise z-maps of regions positively and negatively correlated with the posterior cingulate cortex seed and network (Jenkinson *et al.*, 2012). Contributive effects of WM and CSF regions were negated through including their masks and normalized time series information within the FLAME analysis as regressors. Correction for multiple comparisons was performed on significant clusters through the randomise tool in FSL. Minimum cluster significance was set to $Z > 2.6$ (significance: $p < 0.01$) (Winkler *et al.*, 2014).

5.4 Behavioural Testing

All participants were assessed using Immediate Post Concussion Assessment and Cognitive Testing (ImPACT), Beck Depression Inventory (BDI-II), Short Form Health Survey (SF-36), and the Post Concussion Symptom Scale (PCSS). The ImPACT served to assess memory and reaction times through a series of 6 sub-tests. The ImPACT evaluates several different metrics measuring cognitive efficiency, symptomatology, and overall function. The following list contains each of the different measured scores.

- Symptomatology

- Cognitive efficiency (CE)
- Composite scores:
    1. Verbal memory (VBM)
    2. Visual memory (VIM)
    3. Motor speed (MS)
    4. Reaction time (RT)
    5. Impulse control (IMP)

Higher test scores in the VBM, VIM, and MS scores indicate the subject has increased recall and recognition memory, and processing speed measures. Higher results in these three measures are contiguous with better overall cognitive performance. Lower test scores in the RT, and IMP categories indicate quicker response time, and more well tuned impulse control. Decreases in these measures is also indicative of better cognitive outcome. Greater scores in the symptomatology section indicate more issues with the subject's overall health, and well being. CE is measured through evaluating the relationship between accuracy, and speed on a specific portion of the ImPACT. As such, CE is an indicator of overall cognitive function.

The BDI-II, SF-36, and PCSS tests were used in assessing the subject's mental state, and physical health at the time of the scan. ImPACT, along with the self reported batteries, are used as the basis of a correlation analysis which is described in the following chapter. The BDI-II is a psychometric test focusing specifically on evaluating the subject's mental state. The aim being to evaluate whether depression is present, and measure its severity. SF-36 evaluates a broad range of health criteria.

It offers insight into the athletes mental state, and perception of themself. PCSS evaluates the severity of symptoms commonly found after a concussive injury (irritability, fatigue, emotion, etc.).

5.5 Data Analysis

The data analysis procedure was split into four major studies, all of which are determined through the processing methods described above.

- Case-based study, probing for differences between individual rCFL subjects and the control mean
- Group-based study, investigating broad group changes between the rCFL and control subjects
- Within group study, involving comparisons within the rCFL group, based on different subject criteria (position played, years of professional play and age)
- Correlation analysis between measures of cortical thickness, DTI, fMRI, and behavioural results for each subject

These four methods of comparison were selected as they provide a solid basis for understanding changes in MRI measures for several different scenarios. The case-based study offers individual information on abnormalities for each individual rCFL athlete. This individualized information has been used in reporting study results to each of the recruited athletes. The group-based study allows for the investigation of potentially systematic differences between all rCFL subjects and controls. If the differences are consistent across the rCFL population, it may be possible to attribute

those differences to their years of play in contact sports. The within-group study focuses on identifying potential differences in MRI measures as a result of position played (frequent or less frequent impact), years of professional play (less than or greater than 10 years), or rCFL athlete age (less than or greater than 58 years). The goal of the within-group study is to attribute certain regions or patterns of difference to a subjects career length, choice of position, or age.

5.5.1 Case-Based Study

The case-based portion of this study involved voxel-wise and cluster-based z-scoring techniques for comparison of measures of cortical thickness, DTI metrics, and fMRI connectivity between each individual rCFL athlete and the group of controls. The basic procedure for calculation of z-scores involved subtracting the mean of particular rCFL subject measure (whether it be cortical thickness, FA, fMRI activation, etc.) from the control group mean, and dividing by the control group standard deviation. Z-scores represent how many standard deviations from the group mean a data point would fall along a normal distribution curve, offering information as to significant outliers from the group. The formula used to calculate z-scores is detailed below as Equation 5.1. Relevant measures were tested for Gaussian normal distribution through the computation of skewness and kurtosis measures. This was to ensure statistically proper usage of the z-scoring technique and validate results.

$$Z = \frac{x - \mu}{\sigma} \tag{5.1}$$

In the above equation x is the individual rCFL subject measure being examined, μ is the relevant control group mean for that measure, and σ is the standard deviation

of the control group measure. The goal of this portion of the study was to offer insight as to each individual rCFL ($n = 19$) subject's ranking compared to the control group mean (fCONN fMRI: $n = 19$, ADNI anat: $n = 26$ and ADNI DTI: $n = 29$) for each imaging measure. Z-scores offer a simple, yet robust method of determining significance, as measured through standard deviations from the mean. In this study we have defined outliers as data points which fall at the least $\pm 1.65\sigma$, preferably $\pm 2\sigma$ from the control mean. Due to the inhomogeneity of the individual results, it was decided that a more broad method of results reporting was necessary in order to offer a simple method of ranking each player's individual outcome when compared to control group data. Instead of discussing every region of significant difference for each measure (cortical thickness, fMRI and DTI metrics), a single measure of the number of outlying voxels or clusters ($-2 < z > 2$) is given. Through this methodology, it becomes far easier to identify significant outliers, and perform more advanced correlation analysis. For example, if a rCFL subject has a large number of significantly outlying voxels for all MRI measures, and these correlate with neuropsych evaluations, it becomes easy to to identify them as a potential outlier.

5.5.2 Group-Based Study

The group based study consisted of broad comparisons between all rCFL subjects and controls. Differences between the groups were identified through the use of cluster-based and voxel-wise z-scoring techniques. All comparisons between groups included subject age as a covariate in the analysis procedure. The rCFL population ($n = 19$) was set against the control population (fCONN fMRI: $n = 19$, ADNI anat: $n = 26$ and ADNI DTI: $n = 29$), and regions of group differences were reported for each

imaging metric. Reporting each individual region of difference in the group based study allows for the ability to potentially identify regions which may be systematic outliers in that population. Through identifying common regions of difference across the entire rCFL population, the hope is to label individual regions or structures which may be more susceptible to damage during participation in contact sports.

5.5.3 Within Group Study

The within group study included similar methods of investigation to those described above. A combination of voxel-wise and cluster-based z-scoring was utilized in order to measure within rCFL group differences. Again, individual regions of difference were reported in order to potentially identify systematic differences which could be attributed to the selected rCFL groupings. Specifically, the following differences were investigated:

- rCFL subject age; separate into groups based on age ≤ 58 ($n = 9$, 52.2 ± 4.9 years) or > 58 years ($n = 11$, 62.7 ± 2.2)
- rCFL subject position; separate into groups based on position played, whether it was classified as a frequent contact (on offense: center, running back, full back, guard and tackle, on defense: defensive tackle, linebacker and defensive end) ($n = 13$, 58.2 ± 5.6 years) or less frequent contact position (on offense: quarterback, wide receiver and tight end, on defense: safety and cornerback) ($n = 7$, 57.6 ± 7.6 years)
- rCFL subject length of career; separate into groups based on years of professional play, players whom have participated in ≤ 10 ($n = 11$, 57.7 ± 5.6 years)

or > 10 ($n = 9$, 58.3 ± 7.2 years) seasons of play

5.5.4 Correlating Imaging Measures

Imaging measures and neuropsychological testing results were correlated through calculating the Pearson product moment correlation coefficient r. The goal of these comparisons being to potentially identify connections between changes in imaging measures, and dysfunction in neuropsychiatric testing. The Pearson product moment correlation coefficient offers information as to the the linear correlation between two variables, and is defined as follows in Equation 5.2.

$$r = \frac{\sum x_i y_i - n\bar{x}\bar{y}}{(n-1)s_x s_y} \tag{5.2}$$

Above, n is the number of observations, $\bar{x}$ is the mean of all x_i samples, $\bar{y}$ is the mean of all y_i samples, s_x is the standard deviation for sample x and s_y is the standard deviation for variable y. The Pearson coefficient, r, varies from $-1 \leq r \geq 1$, where -1 indicates a perfect negative linear relationship, 1 indicates a perfect positive relationship, and 0 proposes that there is no correlation. An example of each of the described scenarios is shown in figure 5.8. The relative strength of correlation r can be broken into rough groupings as follows:

- Very weak, weak correlation: $0.00 - 0.19$, $0.20 - 0.39$
- Moderate correlation: $0.40 - 0.59$
- Strong, very strong: $0.60 - 0.79$, $0.80 - 1.00$

For purposes of identifying a relatively strong correlative relationship between results, the strong-very strong bracket was selected ($0.60 < r < 1.00$).

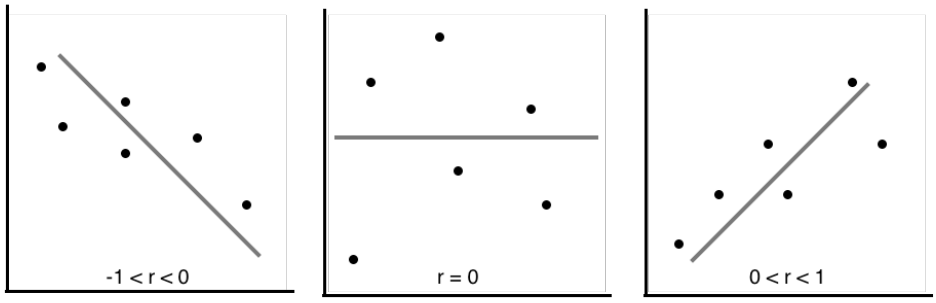

Figure 5.8: Visual examples of the three possible situations for Pearson correlation coefficient r.

Chapter 6

Results and Evaluation

The following section will detail the results of all performed analysis, and provide insight as to their significance in existing literature.

6.1 Behavioural Results

The first data to report, prior to delving into the imaging analysis, are the behavioural testing results. At the time of subject testing the subjects completed the ImPACT, BDI-II, SF-36, and the PCSS. These alone offer important information as to the overall mental, and physical well being of the subjects. Further analysis will probe for any correlation between imaging and behavioural results.

The average BDI-II score of all rCFL subjects was 8.0 ± 6.9. This result straddles the minimal-mild depression boundary (minimal $0-13$, mild $14-19$). The guidelines for assessing depression are as follows:

- $0-13$: minimal depression

- $14 - 19$: mild depression
- $20 - 28$: moderate depression
- $29 - 63$: severe depression

The highest recorded BDI-II score was 25, which places the rCFL subject within the moderate depression category. See table 6.1 for more information on the BDI-II scoring results. Significant increases in the in BDI-II measures were found between the rCFL population and recruited controls ($z = 2.04$). On average, the rCFL population reported almost 4 times greater levels of depression-like symptoms than controls. Previous work has demonstrated that a history of concussive head trauma often correlates with higher incidence of depression (Chrisman and Richardson, 2014; Kontos *et al.*, 2012; Guskiewicz *et al.*, 2007). This correlation becomes stronger as the number of lifetime concussions suffered increases (Didehbani *et al.*, 2013). In addition, Guskiewicz *et al.* reported that those who have suffered only one or two previous concussions were nearly 1.5 times more likely to be diagnosed with depression, and those with 3 or more were 3 times more likely (Guskiewicz *et al.*, 2007).

Table 6.1 also includes results of PCSS testing. On average, rCFL subjects scored more than 4 times the result of the control group ($z = 1.80$). The most frequently high scored categories for rCFL subjects were involving irritability, sadness, difficultly sleeping, sensitivity to light, and difficulty remembering. These symptoms are consistent with the results of previous work (McCrory *et al.*, 2013).

Results of ImPACT computerized testing were not as conclusive as the BDI-II and PCSS scores. There were no significant differences found between the rCFL

Table 6.1: Results BDI-II and PCSS behavioural testing. rCFL players versus recruited controls (used for EEG but not MRI analysis). rCFL players demonstrate higher PCSS and BDI-II measures than controls. This indicating an increase in depression and concussive symptomatology. Bold text indicates significance of that measure ($z > 1.65$).

Behavioural Test	*Control*	*rCFL*
BDI-II	2.39 ± 2.83	8.15 ± 7.03
PCSS	3.11 ± 5.7	13.35 ± 11.98

and control group measures which passed the minimum significance threshold of $z = \pm 1.65\sigma$. This could be in part to the fact that the ImPACT test is designed to be compared to a single subject's data before and after a concussion, not a group comparison on a single occasion. The measure which exhibited the most amount of difference was involving CEI. CEI measures the interaction between accuracy and speed in seconds in the symbol matching test. Accuracy indicating the percentage of correct responses, and speed representing the time to respond. A higher score indicates better performance in both categories. The rCFL population scored very poorly, which could be indicative of potential issues with overall cognitive efficiency. Previous work by Schatz *et al.*, demonstrated impairments in processing speed, visual memory and impulse control in a population of 72 recently concussed high school athletes (Schatz *et al.*, 2006).

The final test performed was the SF-36. The SF-36 consists of self reported questions regarding a vast range of health criteria. It offers insight into the athlete's mental state and perception of themselves. Self-reported social function scores in

Table 6.2: Results of ImPACT computerized testing. rCFL players versus recruited controls (used for EEG but not MRI analysis). rCFL players demonstrate similar measures to those of controls. Lower (but not significant) CEI is observed in rCFL subjects compared to controls.

ImPACT	*Control*	*rCFL*
Verbal Memory	82 ± 10.80	77.35 ± 9.90
Visual Memory	63.83 ± 14.46	63.40 ± 12.08
Motor Speed	34.19 ± 6.95	30.99 ± 4.69
Reaction Time	0.75 ± 0.15	0.78 ± 0.16
Impulse Control	1.44 ± 1.38	1.90 ± 1.45
Cognitive Eff. Index	0.13 ± 1.17	0.04 ± 0.23

rCFL subjects were found to be significantly lower ($z = -3.34$) than controls. Across the entire evaluation, rCFL subjects reported lower overall measures in every category, with the pain category being the next largest discrepancy between control and rCFL groups (after the social function grouping). Lower scores in the SF-36 indicate overall poorer general health in the rCFL group as compared to the control group. Previous work by Guskiewicz et al., reported that in a group of 2552 retired professional football players, those with a history of concussion and depressive episodes also are more likely to experience general pain (muscle and joint) and declining health conditions, as well as a feeling of helplessness towards these changes (Guskiewicz *et al.*, 2007).

Table 6.3: Results of SF-36 behavioural testing. rCFL players versus recruited controls (used for EEG but not MRI analysis). rCFL players demonstrate significantly lower measures in social function, and pain compared to controls.

SF-36	*Control*	*rCFL*
Physical Function	81.94 ± 28.56	78.25 ± 18.73
Limit. d.t. Physical Health	98.61 ± 5.89	88.75 ± 23.01
Limit. d.t Emotional Health	98.15 ± 7.86	81.67 ± 35.71
Energy/Fatigue	70.83 ± 11.79	62.25 ± 19.78
Emotion Well-Being	86.89 ± 6.83	77.8 ± 17.82
Social Function	97.22 ± 5.35	79.36 ± 23.48
Pain	83.89 ± 18.49	61.13 ± 20.19
General Health	79.72 ± 12.77	72.75 ± 15.93

6.2 Case-Based Analysis

6.2.1 Track-based Spatial Statistics

The first study involved applying the processing pipeline to each individual rCFL subject and the group of controls. Using a z-score methodology, significant measures for each imaging metric and each individual subject were extracted. Table 6.4 contains information about voxels which pass a significance threshold of $z \pm 1.65$ for each DTI tensor measure. All data was tested for Gaussian normality through the use of skewness and kurtosis methods. A lower threshold was chosen for DTI significance due to the lack of cluster-based thresholding inference or the threshold-free enhancement methods within the analysis pipeline. Thresholding through a global z-scoring methodology is more stringent than the cluster based or threshold-free methodology, and hence a lower (yet still meaningful) threshold of significance was selected. In addition, only a select few voxels from each white matter tract were selected as part of the tract invariant skeleton for further statistical analysis during the TBSS procedure,

so cluster-based thresholding would yield poor results.

The most commonly reported measures include increased AD in rCFL subjects compared to controls (in 12 of 19 subjects), along with increased MD, and RD in rCFL subjects versus controls (in 7 of 19 subjects). Interestingly, there were mixed results in terms of FA measures. Of the 19 subjects tested, a total of 14 exhibited significantly altered measures of FA. However, of these 14 subjects, half exhibited heightened FA compared to controls while the other half demonstrated decreased FA. This inhomogeneity in tensor measures makes individual results somewhat tricky to interpret. The clearest trend appears to be involving the increased AD measures in rCFL versus controls, with an average of 5836 ± 8415 significant voxels appearing ($n = 12$). Interpretation of these results will become more evident later on in this chapter, as group and within-group comparisons are investigated.

Several of the recruited rCFL subjects exhibited widespread differences in DTI measures. These datasets were further investigated to ensure that there were not any errors that occurred during the processing.

6.2.2 Seed-based Correlation Analysis

The second case-based analysis focused on probing differences in resting state connectivity between each individual rCFL athlete and the control group. Findings are reported as the size of the largest surviving cluster which passed a stringent z-threshold of $\pm 2\sigma$ from the control mean ($-2 < z < 2$). Table 6.5 provides details on the size and location of each outlying cluster significantly above ($z > 2$), and significantly below ($z < -2$) the control group mean. Clusters were reported as opposed to

Table 6.4: Results from the cluster-wise z-scoring seed based ROI analysis. Individual rCFL players were placed against controls, with age as a covariate. Significant results were chosen as results falling $\pm 1.65\sigma$ from the control mean.

(voxels)	*Cntrl*	>	*rCFL*		*rCFL*	>	*Cntrl*	
rCFL Number	*FA*	*MD*	*AD*	*RD*	*FA*	*MD*	*AD*	*RD*
1	46238	-	-	-	-	33890	5788	38869
2	-	-	-	2163	36592	-	15570	-
3	-	-	-	-	9904	-	5246	-
4	-	-	-	-	-	307	980	148
5	6088	-	242	-	-	-	-	-
6	-	-	-	-	-	-	-	354
7	42615	2427	48411	-	-	-	-	-
8	-	-	-	-	1723	-	-	-
9	76	-	-	29	-	3	5	5
10	-	-	-	-	-	-	27194	-
11	-	-	-	-	-	185	15122	-
12	-	-	-	-	-	-	-	-
13	251	-	-	-	-	5	2802	5
14	-	-	-	-	17564	-	231	-
15	-	32	111	12953	2892	-	225	-
16	1382	-	-	-	-	1894	19396	1447
17	516	-	-	-	-	467	18325	348
18	-	72	204	51	160	-	-	-
19	-	-	-	-	582	-	-	-

voxels, as fMRI analysis often is plagued by contributions of noise and motion. Along with the strategies described previously in the Methods section, clustering helps to retain important signal information while also acting to negate the effect of unwanted contributions.

Table 6.5: Results from the cluster-wise z-scoring seed based ROI analysis. Individual rCFL players were placed against controls, with age as a covariate. Significant results were chosen as results falling $\pm 2\sigma$ from the control mean.

rCFL Number	$z < -2$ *(voxels)*	*MNI Coordinates*	$z > 2$ *(voxels)*	*MNI Coordinates*
1	1383	-7, 57, 17	307	-57, -11 -18
2	1004	-5, 45, 17	221	39, -78, -37
3	410	1, -50, 23	457	4, 32, -10
4	505	15, 32, 9	-	-
5	437	-20, 28, 37	2063	1, -63, -54
6	144	3, -50, 24	-	-
7	170	18, 21, 33	-	-
8	149	1, -53, 26	260	-41, 52, -8
9	354	4, 23, 10	102	-11, -56, -60
10	1705	9, 38, 3	167	-15, -64, -57
11	109	-52, 10, 18	331	13, -84, -33
12	249	1, -50, 27	288	-21, -72, -51
13	105	-14, 58, 10	361	-13, 32, -11
14	350	0, -52, 21	159	13, 31, -9
15	11008	2, -60, -16	-	-
16	202	-45, 6, -26	-	-
17	706	4, -49, 19	-	-
18	3592	4, -55, -29	-	-
19	-	-	227	-50, 31, -18

Interestingly, significant negative z-scores (indicating decreased functional connectivity in rCFL subjects compared to controls) were found in larger quantity and larger size than positive z-scores. The average size of the largest cluster in the case of $z < -2$ was 1189 ± 2456 voxels ($n = 18$ significant clusters). For the case where $z > 2$, the average cluster size was 260 ± 448 voxels ($n = 12$ significant clusters). There is significant variation within these results, as is to be expected with seed based ROI analysis. Some of the rCFL subjects exhibited extremely large and significant clusters of hyper or hypo-connectivity. More detail into interpretation of these results follows

in the correlation results with neuropsych testing. The general trend across the entire rCFL population involved alterations in rs-connectivity through increased, as well as decreased activation and recruitment in sections of the DMN.

6.2.3 Cortical Thickness Measures

Next, cortical thickness was evaluated between individual rCFL subjects and controls. The results of this analysis are detailed in table 6.6. In general, the rCFL population demonstrated significant cortical thinning when compared to controls (18 out of 20 players experienced significant regions of thinning). On average, the rCFL population demonstrated 2343 ± 2549 voxels which had significantly lower cortical thickness measures than controls ($z < -2$). Out of the rCFL population, only 4 subjects demonstrated regions of thicker cortical structures when compared to controls (260 ± 449 voxels, $z > 2$). Table 6.6 includes the peak z-score, subject number, and number of significantly outlying voxels. All clusters survived a stringent thresholding of $\pm 2\sigma$ from the control mean, and cluster-wise correction for multiple comparisons. The sum of all significant clusters was computed for subjects who had multiple regions of significant difference.

In the following sections, neuropsychiatric testing and neuroimaging measures will be investigated for any relationships through correlation analysis. Looking for connections among these separate techniques will hopefully allow for the identification of patterns, which may lead to a deeper understanding of individual player outcomes based off of individual metrics.

Table 6.6: Results from correction for multiple comparisons of the voxel-wise cortical thickness measures ($-2 < z < 2$). Individual rCFL subjects were placed against controls, with age as a covariate.

rCFL Number	*Peak -ve z-score*	*Voxels* $z < -2$	*Peak +ve z-score*	*Voxels* $z > 2$
1	-	-	-	-
2	-4.93	497	-	-
3	-2.80	540	-	-
4	-4.57	4,396	-	-
5	-4.18	1,740	-	-
6	-3.24	492	-	-
7	-4.78	1,949	-	-
8	-4.56	639	-	-
9	-5.89	579	-	-
10	-5.53	637	5.80	527
11	-5.76	4,153	-	-
12	-6.86	6,982	-	-
13	-6.17	3,785	-	-
14	-	-	5.51	805
15	-8.83	554	-	-
16	-6.84	6,430	5.37	549
17	-4.42	8,589	-	-
18	-3.74	1,863	-	-
19	-	-	4.97	3,408
20	-5.49	688	-	-

6.3 Group-Based Analysis

6.3.1 Track-based Spatial Statistics

Moving into the group-based segment of the thesis, results are now computed through investigating group mean differences between the rCFL and control population. The first results to report involve TBSS analysis and the probing of DTI metrics. The ICBM-DTI-81 white-matter labels atlas was used to identify 48 individual white

matter structures. It also served as the basis for realizing local differences in voxel-wise FA, MD, AD and RD measures between the rCFL ($n = 19$) and control ($n = 26$) populations (Mori *et al.*, 2005). Regions or clusters along white matter tracts which demonstrated significant deviation ($-3 < z < 3$, corrected for multiple comparisons, including subject age as a covariate) from the respective group control mean were extracted.

The rCFL population, as a whole, exhibited significant increases in measures of FA, MD, and AD as described through group-wise TBSS, and revealed through voxel-wise z-scoring ($z > 3$). Increased measures of FA in rCFL subjects when compared to controls were noted within the body of the corpus callosum and are shown in figure 6.1. Regions of increased MD in rCFL subjects versus controls included the genu of the corpus callosum and left side anterior corona radiata and are included in figure 6.2. Regions of increased AD in rCFL versus controls included the left optic radiation, left anterior corona radiata, left inferior longitudinal fasciculus, and splenium and genu of the corpus callosum, and are visualized in Figure 6.3.

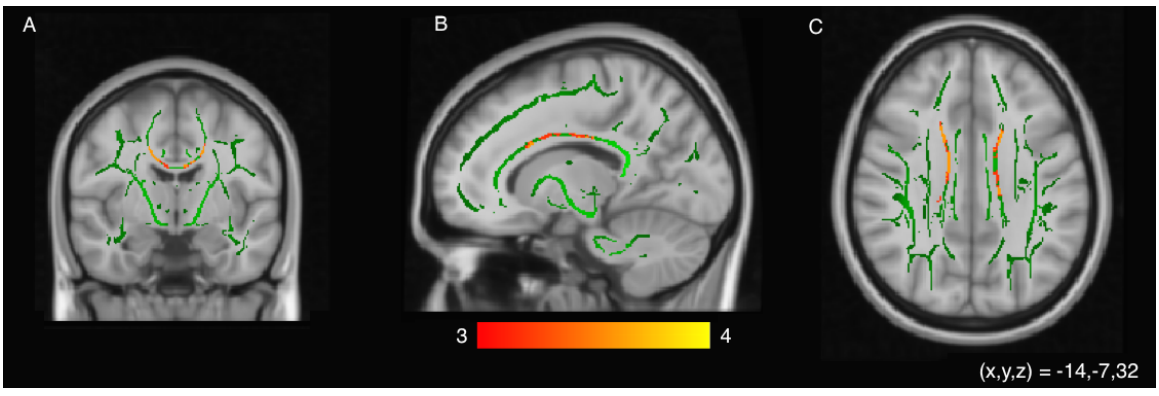

Figure 6.1: DTI TBSS results of FA measure for rCFL group compared to the controls, shown projected onto a standard MNI 1mm template and tract-invariant FA skeleton. Regions appearing in red-yellow indicate a significant increase in that measure ($z > 3$). All images are corrected for multiple comparisons, including age as a covariate.

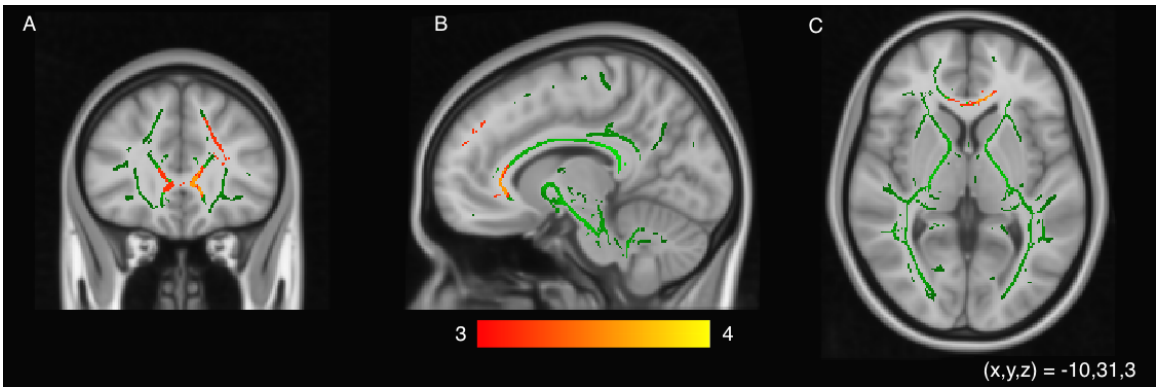

Figure 6.2: DTI TBSS results of MD measures for rCFL group compared to the controls, shown with the same parameters described in Figure 6.1. All images are corrected for multiple comparisons, including age as a covariate.

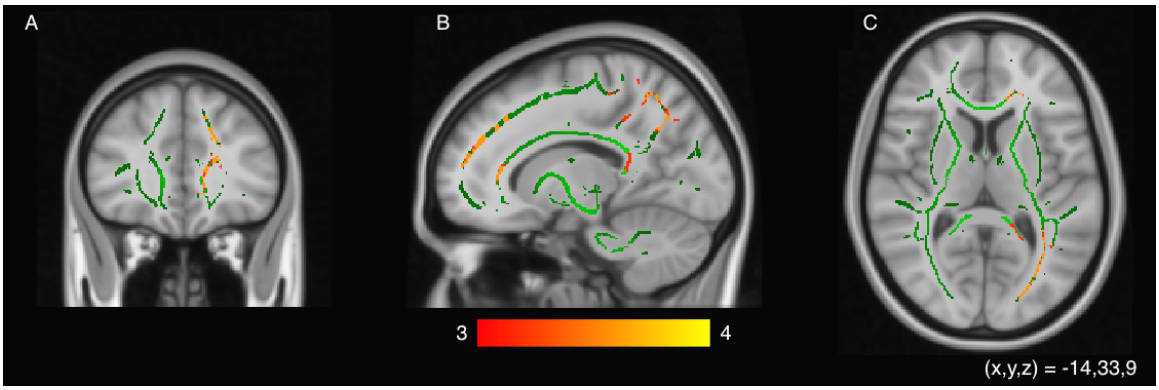

Figure 6.3: DTI TBSS results of AD measures for rCFL group compared to the controls, shown with the same parameters described in Figure 6.1.

The differences detailed above include commissural tracts (connecting the same cortical region within left and right hemispheres), namely the corpus callosum, along with projection tracts (tracts inter-connecting regions of the cortex with other parts of the CNS) such as the left optic radiation and left corona radiata. Prior literature on repetitive sport concussion observed through DTI metrics is somewhat nonuniform. Studies focusing on acute stages of injury (hours to days) often report different results than those focused on subacute stages (first month). Acute studies generally

report increases in FA, thought to be a result of trauma-induced changes in cellular metabolism, which may result in cytotoxic edema (Dimou and Lagopoulos, 2014). Subacute stages on the other hand, report mixed measures of FA, which could be more representative of the complex nature of changes in underlying neuropathology (Dimou and Lagopoulos, 2014).

Our study evaluated rCFL subjects for the effects of sport-related head injury many years (for some players, decades) after suffering a concussion. Sasaki *et al.* evaluated 16 Canadian Interuniversity Sports ice hockey athletes with a history of concussion, compared to 18 Canadian Interuniversity Sports ice hockey athletes without a history of concussion, using a similar DTI processing pipeline (Sasaki *et al.*, 2014). The data acquisition occurred at the end of the season, meaning that the majority of concussed athletes were past the sub-acute (1 month post-injury) phase and into the chronic phase. It was found that the concussed athlete group demonstrated significantly higher measures of FA and AD, and significantly lower measures of RD. Differences in FA measures were mainly localized to association tracts, whereas our results demonstrated an increase in FA within the core of the corpus callosum, involving commissural tracts. Measures of AD aligned with our findings, in that there were significant increases noted in projection fibers, specifically, the corona radiata.

Another more recent study by Multani *et al.* focused on evaluating a population of 18 male retired CFL athletes for damage due to sport-related concussions, comparing them to a group of 17 age-matched healthy controls using DTI metrics (Multani *et al.*, 2016). Similar to our study, it has been many years (even decades) since the retired athlete group's most recent concussion. Findings included significantly increased AD within projection and association fibers, aligning with our results.

The observed differences in MD are somewhat difficult to interpret. Previous work on sport-related concussion and sub-concussive impacts has been somewhat divided between a pattern of increased FA and AD, and decreased MD (Bazarian *et al.*, 2012; McAllister *et al.*, 2012; Davenport *et al.*, 2014; Henry *et al.*, 2011). And a pattern of decreased FA coupled with increased MD and RD (Tremblay *et al.*, 2014; Bazarian *et al.*, 2012). However, the pattern of decreased FA and increased MD is generally more common to findings observed after a TBI, rather than an mTBI or sport-concussion. An explanation for the increased MD noted in our study could be attributed to the late stages of recovery from injury, and introduction of a secondary degenerative mechanism (Tremblay *et al.*, 2014). This secondary, long-term injury mechanism could potentially reverse the effects of the initial inflammatory responses observed in acute and semi-acute phases (decreased MD, with increased FA). These changes could then propagate, presenting many years after the sport-concussions have resided. Our measured increases in MD were found mainly the genu of the corpus callosum. A recent study by Tremblay *et al.* involved probing DTI measures through TBSS on a population of 15 clinically normal, retired athletes with a history of concussions (Tremblay *et al.*, 2014). The group found that aging retired athletes demonstrated decreased FA, along with increased MD and RD, primarily within the fronto-parietal networks, and genu of the corpus callosum.

Increases in AD have previously been thought to indicate axonal degeneration. Effects of axonal degeneration would have compounded over the many years of repetitive sport-related trauma, as axons are a primary site of strain in concussion (Gennarelli *et al.*, 1998). Following a mTBI, axons are in an especially vulnerable state, as a result of disturbances in axoplasmic transport mechanisms (Biasca and Maxwell, 2007;

Gennarelli *et al.*, 1998). Over time, repetitive straining forces may lead to axonal swelling, disruption in transport, and subsequent axonal detachment (Biasca and Maxwell, 2007). The corpus callosum has been previously reported as being especially prone to axonal injury during concussion, and our findings of increased AD within the genu and splenium of the corpus callosum reinforce this claim (Gennarelli *et al.*, 1998).

Our result of increased FA within the central portion (body) of the corpus callosum loosely follows the results of prior work in sport-concussion. Previous work has attributed increased FA in concussed patients (semi-acute to early chronic) in portions of the corpus callosum, to alterations as part of a neuroplastic response to head trauma via up-regulation of active axoplasmic transport (Lipton *et al.*, 2012; Mayer *et al.*, 2010). However, the rCFL population has far exceeded the semi-acute phase of injury, as it has been almost 10 years since a prior injury for many players. Persistent swelling, along with permanent neuroplastic alterations to the corpus callosum could potentially offer an explanation as to to the increased FA measures observed in our work (Sasaki *et al.*, 2014).

6.3.2 Seed-based Correlation Analysis

The next study involved the investigation of group differences between rCFL subjects, and controls. Specifically, probing group differences in the DMN through a seed based correlation analysis, with the seed region in the posterior cingulate cortex. After cluster-wise thresholding with significant results selected as being $\pm 2\sigma$ from the control mean, several differences in connectivity were noted between the populations. The rCFL population exhibited decreased activation within the medial prefrontal

cortex portion of the DMN, when compared with the controls ($z < -2$). The rCFL subjects also demonstrated a small region of increased activation within the posterior cingulate cortex when compared to controls ($z > 2$). Figure 6.5 provides a visual representation of group differences, where the colour bars indicate significance through z-score measures.

The design of a linear model, application of cluster-wise thresholding, and investigation of group differences in functional connectivity between populations offered specific insight into regional differences. Specific regions of difference were highlighted through probing the maps of local network co-activation from the posterior cingulate cortex seed. In figure 6.4, mean activation pathways for the DMN are visualized. Interestingly, when set to the same stringent threshold, the rCFL mean activation pattern does not follow the traditional structure of DMN recruitment. There is a lack of functional recruitment of the frontal portion of the DMN, that being, the medial prefrontal cortex.

Previous work in resting-state fMRI has focused mainly on the sub-acute time frame (1 week, to 1 month post-injury). Within this time frame, there have been general disruptions in functional connectivity observed (Johnson *et al.*, 2012; Zhu *et al.*, 2015). However, some studies also reported no differences in functional organization between injured and control subjects (Zhang *et al.*, 2012). Recently, Churchill *et al.* investigated a group of 22 subjects (21.0 ± 1.7 years) with a history of sport-concussion (average time since most recent concussion was just over 2 years) through resting-state fMRI methods (Churchill *et al.*, 2017). Interestingly, when comparing athletes with and without a history of concussion, they found no significant differences in functional connectivity. However, they did observe a relationship between the

number of concussions suffered, with alterations in functional connectivity observed in the visual and cerebellar regions. In contrast to our findings, we noted significant interruptions within the DMN, with the average time since a previous sport-related concussion approaching more than a decade.

Further investigating the changes commonly observed in the early stages after a sport-concussion, Zhu *et al.* reported in a population of 8 collegiate football athletes (20 ± 1.3 years) significant increases in DMN connectivity (within the posterior cingulate cortex) on the first day after an injury is sustained, significant decreases in DMN integrity after 7 days, and partial recovery of integrity by day 30. The increase in DMN connectivity within the posterior cingulate cortex on the first day post sport-related concussion agrees with our finding of heightened activation within the posterior cingulate cortex in the rCFL population.

It is possible that over the course of their careers, athletes suffered a multitude of sport-related trauma, without time for a full recovery. Over time, alterations to the axonal ions and neurotransmitters of the neurons may have been further exasperated due to these frequent impacts. This could extend the partial recovery time as measured through DMN integrity from 30 days (as reported in Zhu *et al.*) to potentially years, pointing to the interpretation that the rCFL subjects are still in the recovery process.

Recently, Hampshire *et al.* studied a population of 54 NFL alumni aged $20 - 50$ years. The protocol included rigorous neuroimaging and neuropsychological testing, focusing on the performances and brain activation patterns of NFL alumni versus controls (Hampshire *et al.*, 2013). In general, they found hyperactivity in the dorsolateral prefrontal cortex during planning and retrieval tests, along with frontoparietal

hypoconnectivity in NFL alumni when compared to healthy controls. More specifically, significantly reduced functional connectivity within the frontopolar cortex (in NFL alumni compared to controls) was found. This result agrees with our findings of decreased connectivity within frontal cortical regions in rCFL subjects. Hampshire *et al.* also found that the parietal cortex was unaffected in terms of functional connectivity analyses. In our results, the posterior cingulate cortex was found to have increased functional activation when compared to controls. These relatively consistent findings across different study parameters and research institutions could point to hypoactivity in the fronto-polar cortex and medial prefrontal cortex regions as a potential biomarker in the identification of poor outcomes after a history of sport-related concussion.

6.3.3 Cortical Thickness Measures

The final study involved voxel-wise cortical thickness analysis of rCFL subjects, compared to controls. It was revealed that the rCFL subjects as a whole, exihibited significant cortical thinning when compared to controls. In total, 13 specific clusters survived the correction for multiple comparisons ($-2 < z < 2$), all of which are listed in Table 6.7. Regions of cortical thinning included the precuneus, inferior and superior parietal, lateral occipital, caudal middle frontal, inferior and superior temporal, lingual, and paracentral gyri. The regions of grey matter abnormalities can be visualized in figure 6.6. The largest clusters of difference (in terms of size) were in the right temporal lobe, right lingual gyrus, left precuneus, and right pars opercularis.

Recently, Goswami *et al.* studied a population of 22 retired CFL athletes (50 ± 12

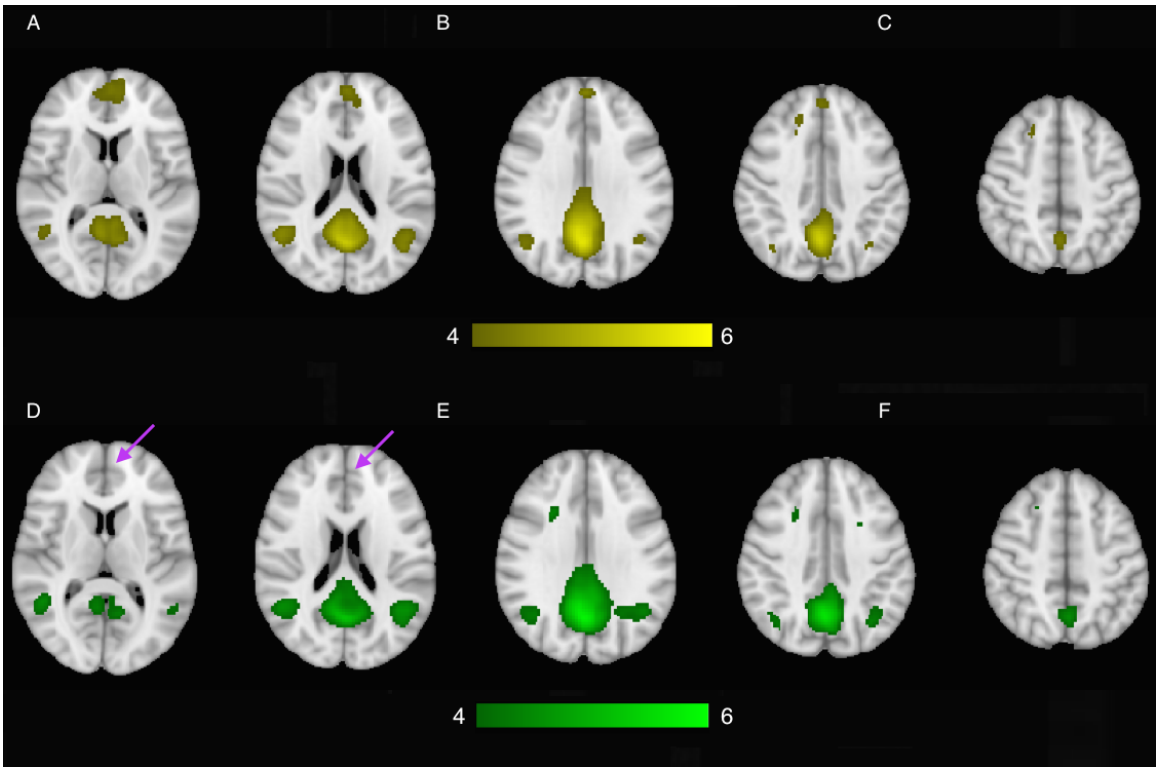

Figure 6.4: Results of rs-fMRI analysis, probing the DMN through seed-based correlation ($4 < z < 6$). The yellow regions indicate mean activation pathways of the DMN for the control population (A-C). Green regions show activation pathways for the rCFL population (D-F). Notice the lack of ventro-medial prefrontal cortex recruitment rCFL population. All images are corrected for multiple comparisons, including age as a covariate.

years) using several MRI techniques, along with behavioural testing and a go/no-go task (Goswami *et al.*, 2016). It was found that when compared to a group of age-matched controls, retired CFL subjects exhibited significant cortical thinning in the anterior temporal lobe (ATL). Our results align with this finding, with the largest region of cortical thinning appearing in the temporal lobe (8809 significantly outlying voxels). The authors go on to suggest a link between behavioural changes (namely aggression and impulsivity) with the health of the UF white matter tract,

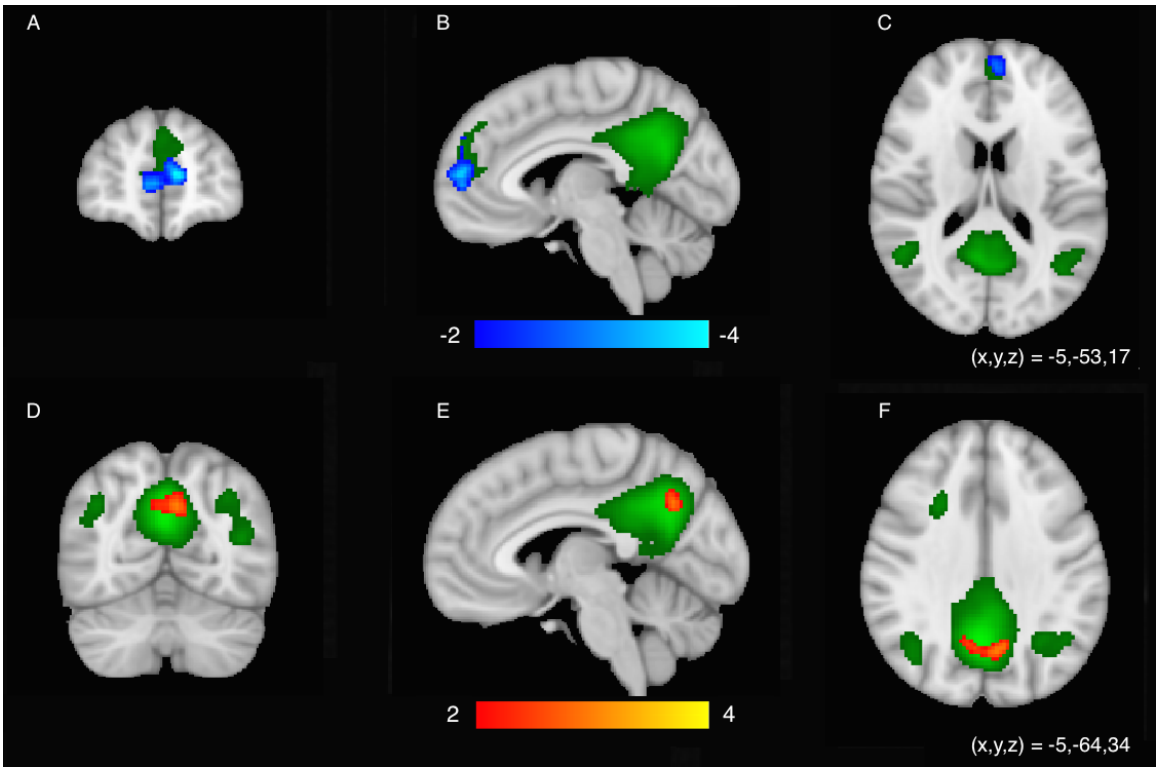

Figure 6.5: Results of rs-fMRI analysis, probing the DMN through seed-based correlation. The green regions indicate mean activation pathways of the DMN for the control (A-C) and rCFL (D-F) populations ($4 < z < 6$). Regions in red-yellow indicate significant increases in network activity in rCFL compared to control populations ($2 < z < 4$), whereas regions in blue-lightblue show significant decreases in activation in rCFL subjects ($-4 < z < -2$). All images are corrected for multiple comparisons, including age as a covariate.

and gray matter regions in the orbitofrontal cortex and anterior temporal lobe. We demonstrated decreased functional connectivity in the frontal pole nearby the location of the orbitofrontal cortex, along with altered AD within the inferior longitudinal fasciculus. It is plausible that a decrease in functional recruitment in the orbitofrontal cortex could be related to the changes observed in cortical thickness in the temporal lobe and altered AD measures within the inferior longitudinal fasciculus.

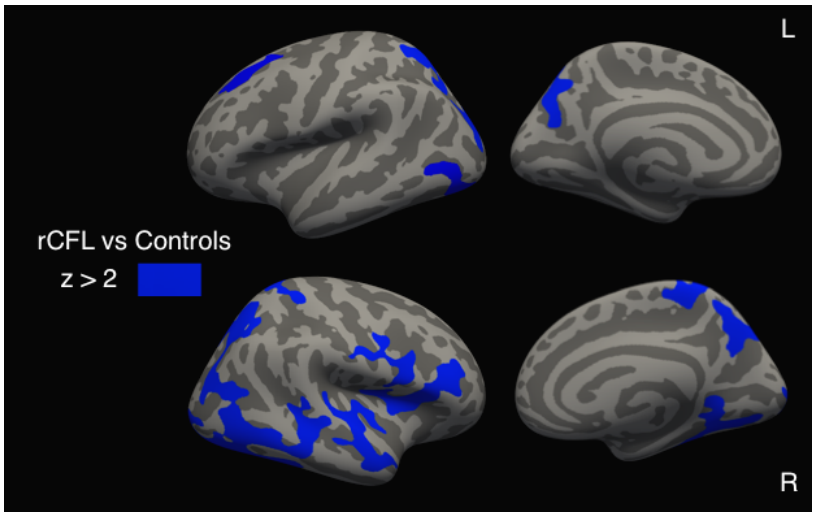

Figure 6.6: Cluster corrected voxel-wise cortical thickness measures comparing rCFL and control groups. Blue regions indicate areas of significant cortical thinning in the rCFL group compared to the controls ($z > 2$).

Another study by Koerte *et al.* focused on examining a group of 15 former professional soccer players (49.3 ± 5.1 years), through cognitive testing, and high resolution T1 mapping (to be used in cortical thickness evaluations) (Koerte *et al.*, 2016). It was found that the retired soccer players exhibited significant cortical thinning within the right inferolateral-parietal, temporal, and occipital cortices when compared with healthy controls. Again, this result agrees with the findings presented in this thesis. More evidence to is required to back up this claim, however, cortical thinning in the temporal lobe (among other regions) could potentially be a common biomarker of repetitive sport-related concussion, regardless of the sport involved.

Looking back at the results of neuropsychological testing, specifically the ImPACT test (the only non-self reported form of testing), the rCFL subjects did not exhibit any significantly different measures when compared to controls. However, while the rCFL population appears normal through ImPACT results, evidence of significant

functional network interruption, altered microstructural integrity, cortical thinning and poor self reported batteries of real life issues, further points to the conclusion that there may be an underlying impairment which is not identified through traditional screening.

Table 6.7: Cluster information from cluster wise correction for multiple comparisons of the voxel wise cortical thickness measures. All rCFL players were placed against controls, with age as a covariate.

Cluster No.	*Voxels*	*MNI Coord. (x,y,z)*	*Peak z-score*	*Region (lobe/gyrus)*
1	1646	-17, -70, 32	3.54	Precuneus L
2	971	-26, -82, 13	3.41	Superior Parietal L
3	875	-37, -79, -14	3.23	Lateral Occipital L
4	747	-27, -82, 13	2.87	Caudal Middle Frontal L
5	547	-39, -80, 6	2.05	Lateral Occipital L
6	7244	43, -61, 0	3.56	Inferior Temporal R
7	1730	25, -5, 0	3.50	Lingual R
8	1663	49, 20, 11	3.42	Pars Opercularis R
9	1565	48, -11, -16	3.36	Superior Temporal R
10	1091	9, -38, 58	3.31	Paracentral R
11	914	43, 4, 22	3.30	Pars Opercularis R
12	575	47, -63, 32	2.12	Inferior Parietal R
13	503	41, -35, 39	1.80	Supramarginal R

6.4 Within-group Analysis

The results of comparisons within the rCFL subject group, based on subject age, position, and number of years played in the CFL are described. Other than the

DTI results discussed below, no other significant differences were observed within the rCFL sub-groupings that exceeded a threshold of $\pm 1.65\sigma$ from the sample mean.

6.4.1 Track-based Spatial Statistics

When looking within the rCFL subject group, there were significant differences observed in all group-wise comparisons performed. Subjects who played in a position where contact was more frequent, exhibited decreased measures of FA within the genu of the corpus callosum when compared with the less-frequent contact group ($z < -1.65$). No other significant differences in MD, AD or RD were noted in the comparison between subject position. Through finite element modeling techniques, the corpus callosum has been found to be the site of consistently high strain in sport related concussion (McAllister *et al.*, 2012). It therefore makes sense to observe altered DTI measures (decreased FA), and presumably decreased microstructural integrity, within the frontal aspect of the corpus callosum in rCFL subjects who played in a frequent contact position.

Increased measures of RD were found in the group of subjects who have played more than 10 seasons professionally ($z > 1.65$). These differences appeared within the body of the corpus callosum, superior corona radiata and superior longitudinal fasciculus. No other significant changes were noted in measures of FA, MD or AD. Visual representations of the within rCFL group differences are shown in figure 6.7.

The greatest (and also most significant) number of differences were observed in the comparison between rCFL subject groups based on age. The older players exhibited significant and diffuse differences in three of four DTI metrics, when compared to the younger population. However, there was only 10 years age difference between

the two group means, leading us to the thought that there potentially may some form of accelerated deterioration in the older athlete population. Diffuse decreases in FA, along with widespread increases in MD and RD were observed in the older rCFL subjects when compared to the younger population. The differences in FA were noted bilaterally in the anterior corona radiata, superior longitudinal fasciculus, optic radiation, external capsule, and the genu and body of the corpus callosum. Increases in MD were observed in right corona radiata, right external capsule, right optic radiations, and the body of the corpus callosum. Increases in RD were observed in similar regions to those described for MD, including the internal capsule, and splenium of corpus callosum.

Generally, decreased FA in a white matter structure is interpreted as decreased integrity within those fibers. It is interesting that the rCFL subjects who have participated in a position which exposes them to more frequent, yet less intense impacts exhibit lower FA measures when compared to the less-frequent group. This result could point towards the conclusion that it is potentially more damaging to have many low-impact incidents (with a small head to head impact just about every play) than it is to have several larger impacts, representative of the typical concussion (as is more likely in less-frequent contact positions). Increased RD measured with increasing professional career length in the CFL is also an interesting observation. RD is typically seen as an indicator of demyelination, an increase in such a measure could point towards compromised myelin integrity. This finding suggests that a longer professional career, involving more potential for sport-related concussion, can potentially lead to increased demyelination of axons when compared to peers with a shorter career length.

Previous work investigating age related changes through DTI metrics has reported a general pattern of decreasing FA, along with increasing MD and RD, with increasing age (Sexton *et al.*, 2014; Sullivan and Pfefferbaum, 2006). These observed patterns of aging traditionally begin to accelerate in subjects as they reach the $50-60$ year old categories (Sexton *et al.*, 2014). However, our findings indicate a very significant decline in fiber integrity as measured through TBSS DTI results between the younger rCFL ($n = 9$, 52.2 ± 4.9) and older rCFL ($n = 11$, 62.7 ± 2.2) subjects. This result could point to accelerated, as well as more pronounced, age-related changes in those who have a history of sport-related concussion.

6.5 Correlating Imaging Measures

The final portion of study included correlating imaging measures (fMRI, DTI, and cortical thickness) with the results of neuropsychological testing (ImPACT, BDI - II, SF - 36, and PCSS). Interestingly, there were no statistically significant correlations found between any of the performed neuropsychological tests ($0.60 \geq r \leq 1.00$). This result speaks to the lack of consistency across several self-reported batteries, as well as the computerized ImPACT, for identification of injuries sustained many years prior. However, there were several strong correlations observed between individual neuropsych test results and DTI imaging measures.

Sensitivity to light scoring within the PCSS symptom score was found to have a strong correlation with decreases in measures of FA through DTI ($r = 0.677$). Scored results of feelings of sadness (also from the PCSS test) were found to have a strong correlation with increases in measures of both MD, and AD ($r = 0.656$, and $r = 0.660$ respectively). In addition, strong correlations were observed between limitations due

to emotional health scoring in the SF - 36, and increases in measures of MD and AD ($r = 0.645$, and $r = 0.648$ respectively).

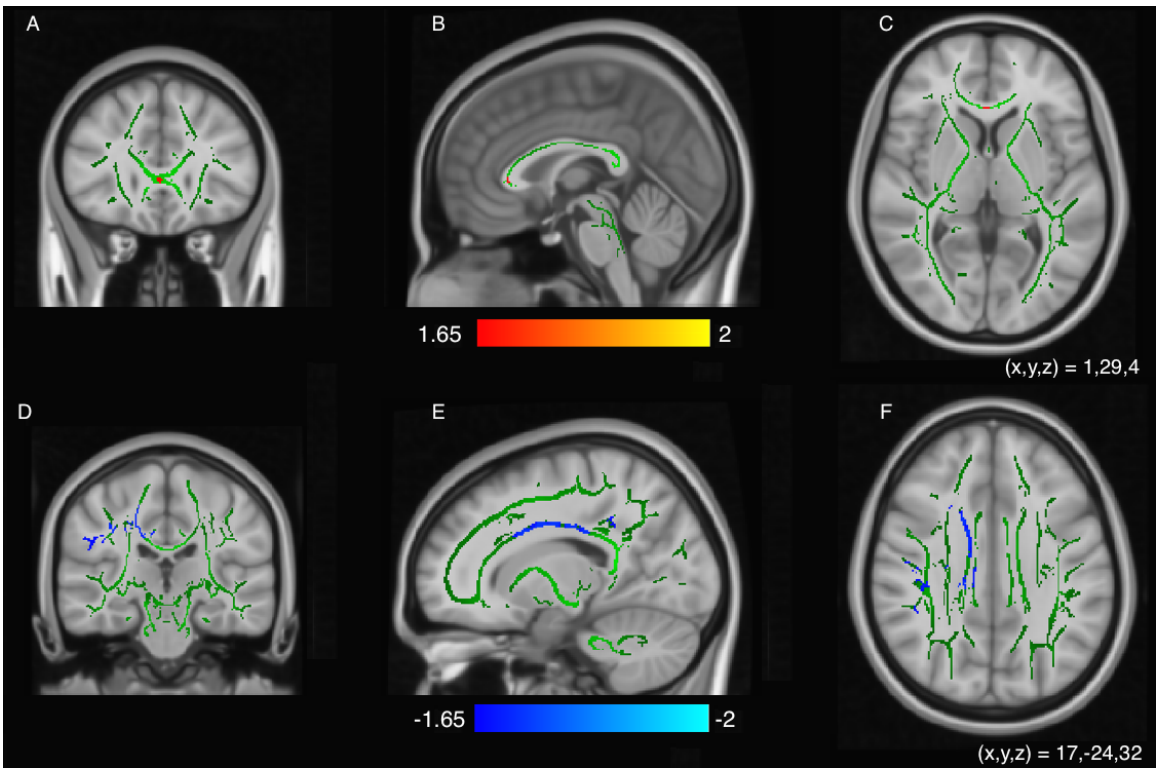

Figure 6.7: Images A, B, and C show frequent versus less-frequent rCFL groups (FA measure). Images D, E, and F show short versus long career length (RD measure). Results are projected onto a standard MNI 1mm template and tract-invariant FA skeleton. Regions appearing in red-yellow indicate a significant increase in that measure ($z > 1.65$), and regions in blue-lightblue indicate a decrease ($z < -1.65$). All images are corrected for multiple comparisons, including age as a covariate. Images A,B and C show regions of higher in FA in the less frequent contact rCFL group when compared to the group of frequent contact athletes. Images D, E and F show areas of lower RD in the athletes with shorter professional careers, compared to those who played for 10 years or longer.

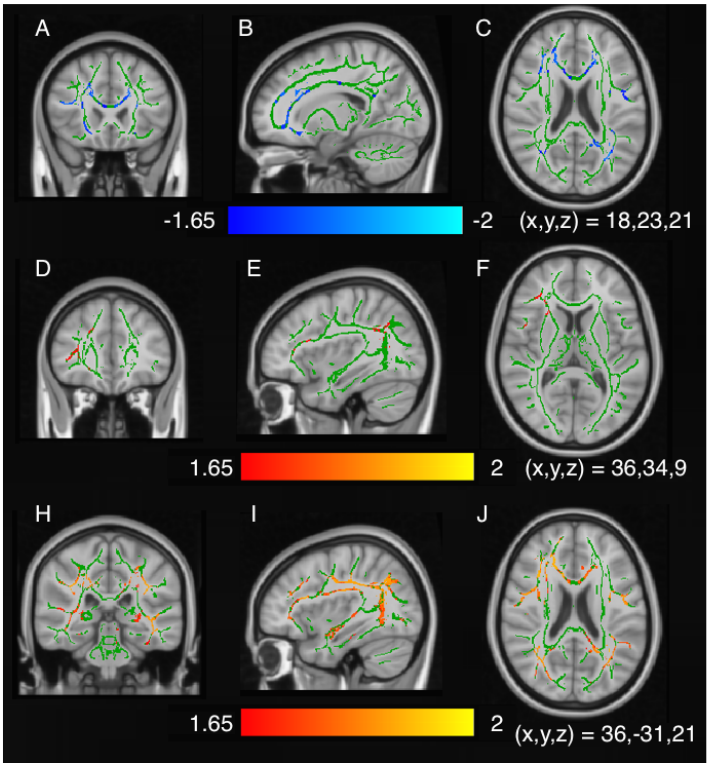

Figure 6.8: DTI TBSS results of the young vs old comparison (age < 58 vs age > 58). Images A, B, and C show lower FA measures in old rCFL subjects ($z < -1.65$, blue-lightblue shading). Images D, E, and F show increased MD measures in the old rCFL group ($z > 1.65$, red-yellow shading). Images H, I, and J detail increases in RD in the old compared to the younger rCFL group ($z > 1.65$, red-yellow shading). All statistical images are shown projected onto a standard MNI 1mm template and tract-invariant FA skeleton.

Chapter 7

Conclusions and Future Work

The following sections will reiterate the findings of this study and provide insight into their significance and relevance. The final section will propose further methods of improvement, and identify analysis techniques which could offer deeper insight in future studies.

7.1 Summary of Major Findings

The long term effects of a career in the CFL were examined through several advanced neuroimaging protocols, and behavioural analyses. There were five main studies within this project, including:

- Behavioural results (BDI-II, PCSS, ImPACT, and SF-36)
- Single rCFL subject compared to controls (DTI, fMRI, anatomical measures)
- Group based comparison, all rCFL compared to controls (DTI, fMRI, anatomical measures)

- Within rCFL group comparison, based on age, length of career and position played (DTI, fMRI, anatomical measures)
- Correlation analyses involving behavioural and neuroimaging results

In this work, we recruited retired athletes of the CFL whom had played a minimum of 3 seasons of professional play. For many of the athletes, it had been greater than a decade since retiring from play, and suffering their last sport-related concussion. Our results, however, point to the discovery that many of these players are still suffering the effects of their concussive past. In the performed behavioural testing, rCFL subjects reported 4 times greater levels of depression (in the BDI-II), as well as 4 times greater levels of symptoms in categories of irritability, sadness, difficulty sleeping, sensitivity to light, and difficutly remembering (in the PCSS) than those without a history of sport-related head injury. In addition, rCFL subjects reported significantly greater pain and reduced social function (in the SF-36) when compared to controls. These figures are truly staggering, and reinforce the idea that all is not well for many of these former athletes.

The results of single subject based neuroimaging analyses confirmed the significant differences detailed in the behavioural results. Significant cortical thinning, along with microstructural anomalies measured through DTI, and functional abnormalities as observed with fMRI were reported. However, when performing correlative analyses, there were no strong correlations observed between any of the behavioural tests, fMRI results or cortical thickness measures. Moderately strong correlation was found between decreased measures of FA in DTI and sensitivity to light as measured by PCSS. Moderately strong correlations were also noted between increases in DTI measures of AD and MD, sadness scoring within the PCSS, and limitations due to

emotional health scoring in the SF-36.

Single subject neuroimaging results yielded varied results. Several rCFL subjects exhibited extreme differences in different specific measures. These extremities were confirmed through repeated analysis to ensure correctness. As a whole there were consistencies in terms of overall changes in MRI measures, but individual regions of damage differed. No strong correlations were found between individual measures of DTI metrics (FA, MD, AD and RD), resting state functional connectivity measured through fMRI, or cortical thickness measures. However, a moderate correlation was observed between the number of functional connectivity anomalies and cortical thinning in rCFL subjects ($r = 0.43$). The inconsistency of inter-subject results and lack of strong correlations with neuropsychological testing speaks to the immense variability of individual neuropathology.

Focusing on group changes observed between the rCFL population and controls allowed for clearer identification of significant regions of difference. A consistent trend of cortical thinning, along with altered functional and microstructural connectivity was noted in retired CFL players. Regions which demonstrated the largest cortical thinning included the temporal lobe, lingual gyrus, precuneus and pars opercularis. The temporal lobe is known to be involved with emotional association and language comprehension. The lingual gyrus functions in vision and processing, and pars opercularis is involved in speech. A decrease in cortical grey matter integrity of the temporal lobe, lingual gyrus, and pars opercularis fits in with the reported decreases in social function, sensitivity to light, and emotional health behavioural scoring in rCFL athletes. The precuneus is heavily involved in episodic memory and reflections of self. Observing a decrease in cortical integrity could be tied into the increased

measures of depression and difficulty with memory reported in rCFL behavioural scores.

Resting-state functional MRI results confirmed the discrepancies observed in cortical thinning measures. Retired CFL players demonstrated decreased functional recruitment within the medial prefrontal cortex, which is a key hub of the DMN. The DMN has many functions, including autobiographical memory. In this memory system, the medial prefrontal cortex is involved with sections of the temporal lobe. Observed decreases in connectivity in frontal regions could tie in with the observed cortical thinning in the anterior temporal lobe.

Finally, DTI measures revealed changes constrained to mainly the corpus callosum, corona radiata, and longitudinal fasiculi. Increased measures of AD and MD point towards potential axonal degeneration due to a history of sport-related concussion. Increased AD has been positively correlated with CSF biomarkers of total tau, and T-tau in healthy subjects with parental history of Alzheimer's disease (Bendlin *et al.*, 2012). Tau deposition is also involved in CTE, so potentially increases in AD along specific regional tracts could be indicative of early signs of CTE. However, to date there have been no studies focusing on the association between repeated sport-concussion, white-matter integrity, and CTE (as CTE is required to be confirmed in autopsy). Interestingly, the corona radiata and longitudinal fasciculi are involved with overall DMN connectivity. The observed interruptions in their microstructural activity could also relate to the observed deficits in functional connectivity.

Potentially the most intriguing results involve comparisons within the retired athlete group. It was found that players who participated in a football position involving more frequent contact demonstrated lower measures of FA within the corpus callosum

when compared to those in less frequent contact positions. Decreased FA is generally an indicator of poorer overall white matter integrity. As mentioned previously, the corpus callosum has been demonstrated to be the primary point of stress in concussion. The finding of decreased corpus callosum integrity in those with more career impacts makes sense. In addition, players whom had played a longer career in the CFL exhibited further signs of white matter damage through increased measures of RD within the body of the corpus callosum, superior corona radiata, and superior longitudinal fasciculus. RD is thought to be an indicator of demyelination, with an increase indicating loss of myelin within those fibers.

In the comparison between rCFL subjects based on age, significant differences in microstructural integrity were observed. The older retired athlete group was found to have decreased measures of FA, along with increased measures of MD and RD. Specific regions of compromised integrity included core regions of white matter, such as the CR, superior LF, optic radiations, external capsule and corpus callosum. Prior work into white matter microstructural integrity and aging has reported similar findings, however, the significance and extent of their findings pale in comparison to those reported here. These findings indicate that the age-related decline observed in athletes whom have suffered multiple sport-related concussions may be significantly sharper in its decline than in healthy subjects.

7.2 Areas of Improvement and Future Work

Moving forward, there are several areas where this study could be improved upon for future work. First and foremost, recording control subject data on the same MRI as recruited subjects would help to remove any small differences in scanning

parameters or site differences. Another useful addition would be to have a clinician or psychiatrist to perform a full medical assessment of each participant, rather than using self-reported metrics. This would help to ensure accuracy and potentially more consistent measures of patient behavioural symptoms.

Performing this study with the inclusion of lifetime data for recruited subjects, in a longitudinal type study would offer significant benefit. Tracking subjects on a yearly basis, beginning at the start of their professional career, and continuing late into life, would provide an incredible depth of information. If it were possible to track an athlete throughout their entire career, the identification of an imaging biomarker for CTE (results could be confirmed in autopsy), along with an identifier for evaluating athlete outcome based on injury history, could be formulated. As of right now there is a significant gap in sport-concussion literature. Many studies report information about athlete outcome days to weeks post injury, with some studies stretching that figure to months. There is a growing body of research involving later-life outcome of sport-related concussion, however, to date there has been no longitudinal study performed across an athletes entire career, and later into life. As a result, we can only infer information about an athletes prior history of injury, without any data to investigate how changes present themselves across their career. In addition, self-reported data on lifetime numbers of concussion are often grossly underestimated. This is due to a lack of knowledge of concussive injury, and the downplaying of injuries in order to remain in the game.

The main questions focused on in a lifetime (or even career) longitudinal study of football athletes would include:

- Do structural anomalies build up over time with more sport-concussions?

- How does the timeline of age-related decline look? Is it similar to that of traditional aging?
- Are patterns of damage in the brain common to impacts of that sport?
- How many sport-concussions until the damage becomes permanent, and potentially chronic?
- Are sub-concussive injuries as damaging as concussive injuries on a long-term basis?

Though these questions are yet to be answered, future longitudinal studies (in excess of $5 - 10$ years) could provide the basis for understanding the potential long-term consequences of concussion. Through furthering our understanding of concussion and the potential long term consequences of injury, the hope is to identify an imaging biomarker for the identification of poor later-life outcome or neurodegenerative disease such as CTE.

Appendix A

Software Algorithms and Scripts

This chapter will detail the software algorithms and scripts utilized in the preparation of this thesis.

A.1 fMRI Processing Pipeline

```
#!/bin/bash

# Follow the procedure outlined in
# Haneef, et al. (2014). Functional connectivity of
# hippocampal networks in temporal lobe epilepsy.
# Epilepsia, 55(1), 137-145.

# If the control and CFL scans aren't in the new directory,
# then create.
[[ -d ${fmri_dir}/ROI_fMRI ]] || mkdir ${fmri_dir}/ROI_fMRI
```

```
# Do the MCFLIRT motion correction (controls and subjects).
cd ${fmri_dir}/ROI_fMRI/Cntrl_RS
for i in cntrl_RS_*.nii.gz; do
[[ -d MCF ]] || mkdir MCF
[[ -f MCF/${i}_mcf.nii.gz ]] || mcflirt -in ${i} -o MCF/${i}_mcf \
&& echo ... running MCFLIRT on $i
done

# Do the BET brain extractions (controls and subjects).
cd ${fmri_dir}/ROI_fMRI/Cntrl_Anat
for i in cntrl_anat_*.nii.gz; do
[[ -d BET ]] || mkdir BET
[[ -f BET/${i}_brain.nii.gz ]] || bet2 ${i} BET/${i}_brain \
&& echo ... running BET on $i
done

# Brain extract the data (controls and subjects).
cd ${fmri_dir}/ROI_fMRI/Cntrl_RS
for i in cntrl_RS_*.nii.gz; do
[[ -d BET ]] || mkdir BET
if [ ! -f "BET/${i}_brain.nii.gz" ]; then
fslsplit MCF/${i}_mcf vol_ -t
for j in vol_*; do
```

```
bet2 ${j} ${j}_brain -f 0.5
done
fslmerge -tr BET/${i}_brain vol_*_brain.nii.gz 2.0
rm -f vol_*
echo ... running BET on $i
fi
done

# Make a text file with all important data (controls and subjects).
cd ${fmri_dir}/ROI_fMRI/Cntrl_Anat/BET
find $PWD -name "*_brain.nii.gz" > cntrl_anat_scans.txt

cd ${fmri_dir}/ROI_fMRI/Cntrl_RS/BET
find $PWD -name "*_brain.nii.gz" > cntrl_RS_scans.txt

# Then run feat_gui, only for pre-stats.
# Used 3 DOF only for CFL data, as well as no transformation.
# Seemed to give the best segmentation results.
# Next, need to use each generated template matrix -
# standard2example_func.mat - to transform CSF and white matter ROI
# into the space of each subject to be later regressed out.
cd ${fmri_dir}/ROI_fMRI/Cntrl_RS/BET
for i in `cat ${fmri_dir}/ROI_fMRI/cntrl_scans.txt`; do
[[ -d ROI ]] || mkdir ROI
```

```
if [ ! -f "${fmri_dir}std_${i}_CSF_reg_thr.nii.gz" ]\
; then

[[ -d ${fmri_dir}/ROI_fMRI/Cntrl_RS/BET/ROI/THR ]] || \
mkdir ${fmri_dir}/ROI_fMRI/Cntrl_RS/BET/ROI/THR
# reg CSF to func
flirt -in ${ROI_dir}/MNI152_T1_0_pve_0_CSF.nii.gz \
-ref filtered_func_data.nii.gz \
-applyxfm -init standard2example_func.mat -out std_${i}_CSF_reg
# threshold CSF to 0.98
fslmaths std_${i}_CSF_reg -thr 0.98 std_${i}_CSF_reg_thr
# reg WM to func
flirt -in MNI152_T1_0_pve_2_WM.nii.gz \
-ref filtered_func_data.nii.gz -applyxfm \
-init standard2example_func.mat -out std_${i}_WM_reg
# threshold WM to 1
fslmaths std_${i}_WM_reg -thr 0.99 std_${i}_WM_reg_thr

fi
echo "... running transformation to functional space for control
image $i"
cd ${fmri_dir}/ROI_fMRI/Cntrl_RS/BET/ROI/THR
fslmeants -i filtered_func_data.nii.gz -o CSF_noise_${i}.txt \
-m std_${i}_CSF_reg_thr
```

```
fslmeants -i filtered_func_data.nii.gz -o WM_noise_${i}.txt \
-m std_${i}_WM_reg_thr
done

# Running the motion regressor stuff (controls and subjects).
cd ${fmri_dir}/ROI_fMRI/Cntrl_RS/BET
for i in `cat ${fmri_dir}/ROI_fMRI/cntrl_scans.txt`; do
if [ ! -f "filtered_func_data.nii.gz" ]; then
cd cntrl_RS_${i}.nii_preproc_cntrl.feat
echo "loop"
echo "${i}"
sed -i "" "s/hold/${i}/g" ${fmri_dir}/ROI_fMRI/Cntrl_Reg_feat.fsf
sed -i "" "s/${i}/hold/g" ${fmri_dir}/ROI_fMRI/Cntrl_Reg_feat.fsf

sed -i "" "s/hold/${i}/g" ${fmri_dir}/ROI_fMRI/Cntrl_Reg_feat.fsf
feat ${fmri_dir}/ROI_fMRI/Cntrl_Reg_feat.fsf
echo "... running feat for regressors for conrtol $i"
sed -i "" "s/${i}/hold/g" ${fmri_dir}/ROI_fMRI/Cntrl_Reg_feat.fsf
fi
done

# Running the normalization stuff - demean the residuals from the
# above output (controls and subjects).
cd ${fmri_dir}/ROI_fMRI/Cntrl_RS/BET
```

```
for i in `cat ${fmri_dir}/ROI_fMRI/cntrl_scans.txt`; do
cd ${fmri_dir}/${i}_motion_reg.feat
if [ ! -f "${fmri_dir}/scaled_fil_func.nii.gz" ]; then
echo "loop"
echo "${i}"
fslmaths filtered_func_data.nii.gz -Tmean mean_fil_func
fslmaths filtered_func_data.nii.gz -Tstd std_fil_func
fslmaths filtered_func_data.nii.gz -sub mean_fil_func.nii.gz \
-div std_fil_func.nii.gz -add 100 -mul mask.nii.gz scaled_fil_func

echo "... running demeaning of residuals for control $i"
fi

if [ ! -f "${fmri_dir}/mean_ts_PCC.txt" ]; then

# Transform the ROI seeds into control subject space
flirt -in ${fmri_dir}/PCC_fMRI/vmPFCsphere.nii.gz \
-ref ${fmri_dir}/mean_func.nii.gz \
-applyxfm -init standard2example_func.mat \
-out ${fmri_dir}/vmPFCsphere_reg

flirt -in ${fmri_dir}/mean_func.nii.gz \
-applyxfm -init ${fmri_dir}/standard2example_func.mat \
-out ${fmri_dir}/PCCsphere_reg
```

```
echo "... running registration of seed ROIs for control $i"

cd ${fmri_dir}/${i}_motion_reg.feat

fslmeants -i filtered_func_data -o mean_ts_vmPFC.txt -m vmPFCsphere_reg
fslmeants -i filtered_func_data -o mean_ts_PCC.txt -m PCCsphere_reg
fi

# Now running partial correlation between seed voxels an other
# brain voxels
# (done separately)
if [ ! -f Par_Corr_${i}.feat/filtered_func_data.nii.gz ]; then
echo "loop"
echo "${i}"
cd ${fmri_dir}/${i}_motion_reg.feat
sed -i "" "s/hold/${i}/g" ${fmri_dir}/Cntrl_ROI_res.fsf
sed -i "" "s/${i}/hold/g" ${fmri_dir}/Cntrl_ROI_res.fsf

sed -i "" "s/hold/${i}/g" ${fmri_dir}/Cntrl_ROI_res.fsf
feat ${fmri_dir}/Cntrl_ROI_res.fsf
echo "... running feat for regressors for patient $i"
sed -i "" "s/${i}/hold/g" ${fmri_dir}/Cntrl_ROI_res.fsf
fi
```

```
# Register the COPE images
cd /Par_Corr_${i}.feat/stats/

flirt -in cope1 -ref $FSLDIR/data/standard/MNI152_T1_2mm_brain.nii.gz \
-applyxfm -init ${fmri_dir}standard2example_func.mat \
-out ${fmri_dir}cope1_reg
done
```

A.2 DTI Processing Pipeline

```
#!/bin/bash

##########################################
# New CFL scan processing and placement
##########################################

echo " "
echo -n "Enter the exam number for the new
CFL patient to process and press [ENTER]: "
read exam_name

# Merge the dti19, dti20 and dti21 files
# and store in dti_merge
# split each file into individual volumes.
```

```
# (ie. 23 for 19-dir, 24 for 20-dir, and
# 25 for 21-dir)
# Want B0 volumes at the start, and B1000
# values afterwards

# Make sure the data is in the proper series'
# 19 dir --> Ser7
# 20 dir --> Ser8
# 21 dir --> Ser9
# Convert data to nifti format and process
cd $data/CFL_Data
mkdir $exam_name

cd $new_data
dcm2niix -z y -o $data/CFL_Data/$exam_name \
-f dti19 $new_data/$exam_name/Ser7

dcm2niix -z y -o $data/CFL_Data/$exam_name \
-f dti20 $new_data/$exam_name/Ser8

dcm2niix -z y -o $data/CFL_Data/$exam_name \
-f dti21 $new_data/$exam_name/Ser9

cd $data/CFL_Data/$exam_name
```

```
mkdir DTI_Merge

# Split the 3 separate DTI scans
fslsplit dti19.nii.gz DTI_Merge/v19_
fslsplit dti20.nii.gz DTI_Merge/v20_
fslsplit dti21.nii.gz DTI_Merge/v21_
echo "Done splitting files "

cd $data/CFL_Data/$exam_name/DTI_Merge
mkdir Results

# Merge the split DTI scans in the proper
# order for processing
fslmerge -t dti60.nii \
v19_0000 v19_0001 v19_0012 v19_0022 \
v20_0000 v20_0001 v20_0012 v20_0023 \
v21_0000 v21_0001 v21_0012 v21_0024 \
v19_0002 v19_0003 v19_0004 v19_0005 \
v19_0006 v19_0007 v19_0008 v19_0009 \
v19_0010 v19_0011 v19_0013 v19_0014 \
v19_0015 v19_0016 v19_0017 v19_0018 \
v19_0019 v19_0020 v19_0021 v20_0002 \
v20_0003 v20_0004 v20_0005 v20_0006 \
v20_0007 v20_0008 v20_0009 v20_0010 \
```

```
v20_0011 v20_0013 v20_0014 v20_0015 \
v20_0016 v20_0017 v20_0018 v20_0019 \
v20_0020 v20_0021 v20_0022 v21_0002 \
v21_0003 v21_0004 v21_0005 v21_0006 \
v21_0007 v21_0008 v21_0009 v21_0010 \
v21_0011 v21_0013 v21_0014 v21_0015 \
v21_0016 v21_0017 v21_0018 v21_0019 \
v21_0020 v21_0021 v21_0022 v21_0023
echo "Done merging files "

# Check that the volumes are in the
# correct order/number (12 B0's and
# 60 B1000's), now perform
# a brain extraction using BET.
# S.M. Smith. Fast robust automated
# brain extraction.
# Human Brain Mapping, 17(3):143-155,
# November 2002.
cd DTI_Merge/Results
bet2 dti60.nii.gz dti60_ns -m
echo "Done brain extraction "

# Eddy current correction using FDT
# Diffusion - default volume reference = 0
```

```
cd Results
eddy_correct dti60.nii.gz dti60_corr \
-def trilinear
echo "Done eddy current correction "

# Reconstruct diffusion tensor using
# FDT on the data that has been
# pre-processed (brain extracted) and
# eddy current corrected data
cd $data
cp -R dti60.bvec dti60.bval Results

cd Results
dtifit \
-k dti60_corr.nii.gz \
-o dti60_corr_final     \
-m dti60_ns_mask.nii.gz          \
-r dti60.bvec                    \
-b dti60.bval
echo "Done reconstructing
diffusion tensors "
echo " "

# Calculate the RD image L2+L3/2 from
```

```
# the fit diffusion tensors
cd Results
fslmaths dti60_corr_final_L2.nii.gz \
-add dti60_corr_final_L3.nii.gz sum
fslmaths sum.nii.gz \
-div 2 dti60_corr_final_RD

# Now move the data to the analysis
# location and put in their respective
# folders
cd Results
cp -R dti60_corr_final_FA.nii.gz \
patient_dti_${exam_name}.nii.gz

cp -R dti60_corr_final_L1.nii.gz \
AD/patient_dti_${exam_name}.nii.gz

cp -R dti60_corr_final_MD.nii.gz \
MD/patient_dti_${exam_name}.nii.gz

cp -R dti60_corr_final_RD.nii.gz \
RD/patient_dti_${exam_name}.nii.gz

echo "Done pre-processing of the
```

```
patient_exam_$exam_name._"
fi


##############################
# Re-running the TBSS stuff
# for the new CFL patient
##############################
yes=1
if [ $yes = $full_process ]; then

# TBSS Stage 1, pre-processing
cd $data_TBSS/Redo
tbss_1_preproc *.nii.gz

# TBSS Stage 2, registration
cd $data_TBSS/Redo
tbss_2_reg -T

# TBSS Stage 3, post-registration
# stuff
cd $data_TBSS/Redo
tbss_3_postreg -S
```

```
# TBSS Stage 4, pre-stats
cd $data_TBSS/Redo
######################
## Changed to 0.05
######################
tbss_4_prestats 0.2

# View data with
cd $data_TBSS/stats
fslview all_FA -b 0,0.8 mean_FA_skeleton \
-b 0.2,0.8 -l Green

# TBSS Stage 4
# How many controls, how many patients
# (22 controls, 10 patients so far)
# Design the 2 sample unpaired t-test
# for use in comparison
cd $data_TBSS/Redo/stats
design_ttest2 CFL $controls $patients -m

# Setting up the 2 sample unpaired ttest,
# make sure ALL controls come before the
# patients (alphabetically in the finder)
cd $data_TBSS/Redo/stats
```

```
randomise -i all_FA_skeletonised -o TBSS_FA \
-m mean_FA_skeleton_mask \
-d all_cntrls_vs_rCFL_ageCov.mat \
-t $data_TBSS/Redo/all_cntrls_vs_rCFL_ageCov.con \
-n 500 -v 5 --T2

echo "Done calculating TBSS for FA ... "



# TBSS for non-FA measures
# Axial diffusivity
cd $data_TBSS/Redo
#tbss_non_FA AD

cd $data_TBSS/Redo/stats
randomise -i all_AD_skeletonised -o TBSS_AD \
-m mean_FA_skeleton_mask \
-d all_cntrls_vs_rCFL_ageCov.mat \
-t all_cntrls_vs_rCFL_ageCov.con \
-n 500 -v 5 --T2

echo "Done calculating TBSS for AD ... "

# Mean diffusivity
```

```
cd $data_TBSS/Redo
#tbss_non_FA MD

cd $data_TBSS/Redo/stats
randomise -i all_MD_skeletonised -o TBSS_MD \
 -m mean_FA_skeleton_mask \
 -d all_cntrls_vs_rCFL_ageCov.mat \
 -t all_cntrls_vs_rCFL_ageCov.con \
 -n 500 -v 5 --T2

echo "Done calculating TBSS for MD ... "

# Radial diffusivity
cd $data_TBSS/Redo
#tbss_non_FA RD

cd $data_TBSS/Redo/stats
randomise -i all_RD_skeletonised \
-o TBSS_RD -m mean_FA_skeleton_mask \
-d all_cntrls_vs_rCFL_ageCov.mat \
-t all_cntrls_vs_rCFL_ageCov.con \
-n 500 -v 5 --T2

echo "Done calculating TBSS for RD ... "
```

Bibliography

Andersson, J. L. and Sotiropoulos, S. N. (2016). An integrated approach to correction for off-resonance effects and subject movement in diffusion mr imaging. *Neuroimage*, **125**, 1063–1078.

Barkhoudarian, G., Hovda, D. A., and Giza, C. C. (2011). The molecular pathophysiology of concussive brain injury. *Clinics in sports medicine*, **30**(1), 33–48.

Baugh, C. M., Stamm, J. M., Riley, D. O., Gavett, B. E., Shenton, M. E., Lin, A., Nowinski, C. J., Cantu, R. C., McKee, A. C., and Stern, R. A. (2012). Chronic traumatic encephalopathy: neurodegeneration following repetitive concussive and subconcussive brain trauma. *Brain imaging and behavior*, **6**(2), 244–254.

Bazarian, J. J., Zhu, T., Blyth, B., Borrino, A., and Zhong, J. (2012). Subject-specific changes in brain white matter on diffusion tensor imaging after sports-related concussion. *Magnetic resonance imaging*, **30**(2), 171–180.

Belanger, H. G., Vanderploeg, R. D., Curtiss, G., and Warden, D. L. (2007). Recent neuroimaging techniques in mild traumatic brain injury. *The Journal of neuropsychiatry and clinical neurosciences*, **19**(1), 5–20.

Bendlin, B. B., Carlsson, C. M., Johnson, S. C., Zetterberg, H., Blennow, K., Willette,

A. A., Okonkwo, O. C., Sodhi, A., Ries, M. L., Birdsill, A. C., *et al.* (2012). Csf t-tau/aβ42 predicts white matter microstructure in healthy adults at risk for alzheimers disease. *PloS one*, **7**(6), e37720.

Bernstein, M. A., King, K. F., and Zhou, X. J. (2004). *Handbook of MRI pulse sequences*. Elsevier.

Biasca, N. and Maxwell, W. L. (2007). Minor traumatic brain injury in sports: a review in order to prevent neurological sequelae. *Progress in brain research*, **161**, 263–291.

Bigler, E. D. (2004). Neuropsychological results and neuropathological findings at autopsy in a case of mild traumatic brain injury. *Journal of the International Neuropsychological Society*, **10**(05), 794–806.

Casson, I. R., Viano, D. C., Haacke, E. M., Kou, Z., and LeStrange, D. G. (2014). Is there chronic brain damage in retired nfl players? neuroradiology, neuropsychology, and neurology examinations of 45 retired players. *Sports health*, **6**(5), 384–395.

Chrisman, S. P. and Richardson, L. P. (2014). Prevalence of diagnosed depression in adolescents with history of concussion. *Journal of Adolescent Health*, **54**(5), 582–586.

Churchill, N., Hutchison, M. G., Leung, G., Graham, S., and Schweizer, T. A. (2017). Changes in functional connectivity of the brain associated with a history of sport concussion: A preliminary investigation. *Brain injury*, **31**(1), 39–48.

Davenport, E. M., Whitlow, C. T., Urban, J. E., Espeland, M. A., Jung, Y., Rosenbaum, D. A., Gioia, G. A., Powers, A. K., Stitzel, J. D., and Maldjian, J. A. (2014).

Abnormal white matter integrity related to head impact exposure in a season of high school varsity football. *Journal of neurotrauma*, **31**(19), 1617–1624.

Didehbani, N., Munro Cullum, C., Mansinghani, S., Conover, H., and Hart, J. (2013). Depressive symptoms and concussions in aging retired nfl players. *Archives of clinical neuropsychology*, **28**(5), 418–424.

Dimou, S. and Lagopoulos, J. (2014). Toward objective markers of concussion in sport: a review of white matter and neurometabolic changes in the brain after sports-related concussion. *Journal of neurotrauma*, **31**(5), 413–424.

Ford, J. H., Giovanello, K. S., and Guskiewicz, K. M. (2013). Episodic memory in former professional football players with a history of concussion: an event-related functional neuroimaging study. *Journal of neurotrauma*, **30**(20), 1683–1701.

Gavett, B. E., Stern, R. A., and McKee, A. C. (2011). Chronic traumatic encephalopathy: a potential late effect of sport-related concussive and subconcussive head trauma. *Clinics in sports medicine*, **30**(1), 179–188.

Gennarelli, T. A., Thibault, L. E., and Graham, D. I. (1998). Diffuse axonal injury: an important form of traumatic brain damage. *The Neuroscientist*, **4**(3), 202–215.

Giza, C. C. and Hovda, D. A. (2014). The new neurometabolic cascade of concussion. *Neurosurgery*, **75**(suppl_4), S24–S33.

Goswami, R., Dufort, P., Tartaglia, M., Green, R., Crawley, A., Tator, C., Wennberg, R., Mikulis, D., Keightley, M., and Davis, K. D. (2016). Frontotemporal correlates of impulsivity and machine learning in retired professional athletes with a history of multiple concussions. *Brain structure & function*, **221**, 1911.

Guskiewicz, K. M., Marshall, S. W., Bailes, J., McCrea, M., Harding, H. P., Matthews, A., Mihalik, J. R., and Cantu, R. C. (2007). Recurrent concussion and risk of depression in retired professional football players. *Medicine and science in sports and exercise*, **39**(6), 903.

Hampshire, A., MacDonald, A., and Owen, A. M. (2013). Hypoconnectivity and hyperfrontality in retired american football players. *Scientific Reports (Nature Publisher Group)*, **3**, 2972.

Haneef, Z., Lenartowicz, A., Yeh, H. J., Engel Jr, J., and Stern, J. M. (2014). Network analysis of the default mode network using functional connectivity mri in temporal lobe epilepsy. *JoVE (Journal of Visualized Experiments)*, (90), e51442–e51442.

Hart, J., Kraut, M. A., Womack, K. B., Strain, J., Didehbani, N., Bartz, E., Conover, H., Mansinghani, S., Lu, H., and Cullum, C. M. (2013). Neuroimaging of cognitive dysfunction and depression in aging retired national football league players: a cross-sectional study. *JAMA neurology*, **70**(3), 326–335.

Hendelman, W. (2015). *Atlas of functional neuroanatomy*. CRC press.

Henry, L. C., Tremblay, J., Tremblay, S., Lee, A., Brun, C., Lepore, N., Theoret, H., Ellemberg, D., and Lassonde, M. (2011). Acute and chronic changes in diffusivity measures after sports concussion. *Journal of neurotrauma*, **28**(10), 2049–2059.

Hootman, J. M., Dick, R., and Agel, J. (2007). Epidemiology of collegiate injuries for 15 sports: summary and recommendations for injury prevention initiatives. *Journal of athletic training*, **42**(2), 311.

Jack, C. R., Bernstein, M. A., Fox, N. C., Thompson, P., Alexander, G., Harvey, D., Borowski, B., Britson, P. J., L Whitwell, J., Ward, C., *et al.* (2008). The alzheimer's disease neuroimaging initiative (adni): Mri methods. *Journal of magnetic resonance imaging*, **27**(4), 685–691.

Jenkinson, M., Bannister, P., Brady, M., and Smith, S. (2002). Improved optimization for the robust and accurate linear registration and motion correction of brain images. *Neuroimage*, **17**(2), 825–841.

Jenkinson, M., Pechaud, M., and Smith, S. (2005). Bet2: Mr-based estimation of brain, skull and scalp surfaces. In *Eleventh annual meeting of the organization for human brain mapping*, volume 17, page 167. Toronto.

Jenkinson, M., Beckmann, C. F., Behrens, T. E., Woolrich, M. W., and Smith, S. M. (2012). Fsl. *Neuroimage*, **62**(2), 782–790.

Johansen-Berg, H., Behrens, T., Robson, M., Drobnjak, I., Rushworth, M., Brady, J., Smith, S., Higham, D., and Matthews, P. (2004). Changes in connectivity profiles define functionally distinct regions in human medial frontal cortex. *Proceedings of the National Academy of Sciences of the United States of America*, **101**(36), 13335–13340.

Johnson, B., Zhang, K., Gay, M., Horovitz, S., Hallett, M., Sebastianelli, W., and Slobounov, S. (2012). Alteration of brain default network in subacute phase of injury in concussed individuals: resting-state fmri study. *Neuroimage*, **59**(1), 511–518.

Koerte, I. K., Mayinger, M., Muehlmann, M., Kaufmann, D., Lin, A. P., Steffinger,

D., Fisch, B., Rauchmann, B.-S., Immler, S., Karch, S., *et al.* (2016). Cortical thinning in former professional soccer players. *Brain imaging and behavior*, **10**(3), 792–798.

Kontos, A. P., Covassin, T., Elbin, R., and Parker, T. (2012). Depression and neurocognitive performance after concussion among male and female high school and collegiate athletes. *Archives of physical medicine and rehabilitation*, **93**(10), 1751–1756.

Langlois, J. A., Rutland-Brown, W., and Wald, M. M. (2006). The epidemiology and impact of traumatic brain injury: a brief overview. *The Journal of head trauma rehabilitation*, **21**(5), 375–378.

Lipton, M. L., Kim, N., Park, Y. K., Hulkower, M. B., Gardin, T. M., Shifteh, K., Kim, M., Zimmerman, M. E., Lipton, R. B., and Branch, C. A. (2012). Robust detection of traumatic axonal injury in individual mild traumatic brain injury patients: intersubject variation, change over time and bidirectional changes in anisotropy. *Brain imaging and behavior*, pages 1–14.

MacFarlane, M. P. and Glenn, T. C. (2015). Neurochemical cascade of concussion. *Brain injury*, **29**(2), 139–153.

Marar, M., McIlvain, N. M., Fields, S. K., and Comstock, R. D. (2012). Epidemiology of concussions among united states high school athletes in 20 sports. *The American journal of sports medicine*, **40**(4), 747–755.

Martland, H. S. (1928). Punch drunk. *Journal of the American Medical Association*, **91**(15), 1103–1107.

Mayer, A., Ling, J., Mannell, M., Gasparovic, C., Phillips, J., Doezema, D., Reichard, R., and Yeo, R. (2010). A prospective diffusion tensor imaging study in mild traumatic brain injury. *Neurology*, **74**(8), 643–650.

McAllister, T. W., Ford, J. C., Ji, S., Beckwith, J. G., Flashman, L. A., Paulsen, K., and Greenwald, R. M. (2012). Maximum principal strain and strain rate associated with concussion diagnosis correlates with changes in corpus callosum white matter indices. *Annals of biomedical engineering*, **40**(1), 127–140.

McCrory, P., Meeuwisse, W., Aubry, M., Cantu, B., Dvorak, J., Echemendia, R., Engebretsen, L., Johnston, K., Kutcher, J., Raftery, M., *et al.* (2013). Consensus statement on concussion in sportthe 4th international conference on concussion in sport held in zurich, november 2012. *Journal of science and medicine in sport*, **16**(3), 178–189.

McDonald, B. C., Saykin, A. J., and McAllister, T. W. (2012). Functional mri of mild traumatic brain injury (mtbi): progress and perspectives from the first decade of studies. *Brain imaging and behavior*, **6**(2), 193–207.

McKee, A. C., Cantu, R. C., Nowinski, C. J., Hedley-Whyte, E. T., Gavett, B. E., Budson, A. E., Santini, V. E., Lee, H.-S., Kubilus, C. A., and Stern, R. A. (2009). Chronic traumatic encephalopathy in athletes: progressive tauopathy after repetitive head injury. *Journal of Neuropathology & Experimental Neurology*, **68**(7), 709–735.

Mennes, M., Biswal, B. B., Castellanos, F. X., and Milham, M. P. (2013). Making data sharing work: the fcp/indi experience. *Neuroimage*, **82**, 683–691.

Misc (2017). Sharcnet: a consortium of 18 colleges, universities and research institutes operating a network of high-performance computer clusters across south western, central and northern ontario.

Mori, S., Wakana, S., Van Zijl, P. C., and Nagae-Poetscher, L. (2005). *MRI atlas of human white matter*. Elsevier.

Multani, N., Goswami, R., Khodadadi, M., Ebraheem, A., Davis, K. D., Tator, C. H., Wennberg, R., Mikulis, D. J., Ezerins, L., and Tartaglia, M. C. (2016). The association between white-matter tract abnormalities, and neuropsychiatric and cognitive symptoms in retired professional football players with multiple concussions. *Journal of neurology*, **263**(7), 1332–1341.

Nowinski, W. L. (2011). Introduction to brain anatomy. In *Biomechanics of the Brain*, pages 5–40. Springer.

Omalu, B. I., DeKosky, S. T., Minster, R. L., Kamboh, M. I., Hamilton, R. L., and Wecht, C. H. (2005). Chronic traumatic encephalopathy in a national football league player. *Neurosurgery*, **57**(1), 128–134.

R Core Team (2013). *R: A Language and Environment for Statistical Computing*. R Foundation for Statistical Computing, Vienna, Austria. ISBN 3-900051-07-0.

Rosenthal, J. A., Foraker, R. E., Collins, C. L., and Comstock, R. D. (2014). National high school athlete concussion rates from 2005-2006 to 2011-2012. *The American journal of sports medicine*, **42**(7), 1710–1715.

Sasaki, T., Pasternak, O., Mayinger, M., Muehlmann, M., Savadjiev, P., Bouix, S., Kubicki, M., Fredman, E., Dahlben, B., Helmer, K. G., *et al.* (2014). Hockey

concussion education project, part 3. white matter microstructure in ice hockey players with a history of concussion: a diffusion tensor imaging study. *Journal of neurosurgery*, **120**(4), 882–890.

Schatz, P., Pardini, J. E., Lovell, M. R., Collins, M. W., and Podell, K. (2006). Sensitivity and specificity of the impact test battery for concussion in athletes. *Archives of Clinical Neuropsychology*, **21**(1), 91–99.

Sexton, C. E., Walhovd, K. B., Storsve, A. B., Tamnes, C. K., Westlye, L. T., Johansen-Berg, H., and Fjell, A. M. (2014). Accelerated changes in white matter microstructure during aging: a longitudinal diffusion tensor imaging study. *Journal of Neuroscience*, **34**(46), 15425–15436.

Shenton, M. E., Hamoda, H., Schneiderman, J., Bouix, S., Pasternak, O., Rathi, Y., Vu, M.-A., Purohit, M. P., Helmer, K., Koerte, I., *et al.* (2012). A review of magnetic resonance imaging and diffusion tensor imaging findings in mild traumatic brain injury. *Brain imaging and behavior*, **6**(2), 137–192.

Smith, S. M., Jenkinson, M., Johansen-Berg, H., Rueckert, D., Nichols, T. E., Mackay, C. E., Watkins, K. E., Ciccarelli, O., Cader, M. Z., Matthews, P. M., *et al.* (2006). Tract-based spatial statistics: voxelwise analysis of multi-subject diffusion data. *Neuroimage*, **31**(4), 1487–1505.

Soares, J. M., Marques, P., Alves, V., and Sousa, N. (2013). A hitchhiker's guide to diffusion tensor imaging. *Frontiers in neuroscience*, **7**.

Stern, R. A., Riley, D. O., Daneshvar, D. H., Nowinski, C. J., Cantu, R. C., and

McKee, A. C. (2011). Long-term consequences of repetitive brain trauma: chronic traumatic encephalopathy. *Pm&r*, **3**(10), S460–S467.

Sullivan, E. V. and Pfefferbaum, A. (2006). Diffusion tensor imaging and aging. *Neuroscience & Biobehavioral Reviews*, **30**(6), 749–761.

Talavage, T. M., Nauman, E. A., Breedlove, E. L., Yoruk, U., Dye, A. E., Morigaki, K. E., Feuer, H., and Leverenz, L. J. (2014). Functionally-detected cognitive impairment in high school football players without clinically-diagnosed concussion. *Journal of neurotrauma*, **31**(4), 327–338.

Tartaglia, M. C., Hazrati, L.-N., Davis, K. D., Green, R. E., Wennberg, R., Mikulis, D., Ezerins, L. J., Keightley, M., and Tator, C. (2014). Chronic traumatic encephalopathy and other neurodegenerative proteinopathies. *Frontiers in human neuroscience*, **8**, 30.

Tremblay, S., De Beaumont, L., Henry, L. C., Boulanger, Y., Evans, A. C., Bourgouin, P., Poirier, J., Théoret, H., and Lassonde, M. (2012). Sports concussions and aging: a neuroimaging investigation. *Cerebral cortex*, **23**(5), 1159–1166.

Tremblay, S., Henry, L. C., Bedetti, C., Larson-Dupuis, C., Gagnon, J.-F., Evans, A. C., Théoret, H., Lassonde, M., and Beaumont, L. D. (2014). Diffuse white matter tract abnormalities in clinically normal ageing retired athletes with a history of sports-related concussions. *Brain*, **137**(11), 2997–3011.

Uddin, L. Q., Clare Kelly, A., Biswal, B. B., Xavier Castellanos, F., and Milham, M. P. (2009). Functional connectivity of default mode network components: correlation, anticorrelation, and causality. *Human brain mapping*, **30**(2), 625–637.

Wilde, E., McCauley, S., Hunter, J., Bigler, E., Chu, Z., Wang, Z., Hanten, G., Troyanskaya, M., Yallampalli, R., Li, X., *et al.* (2008). Diffusion tensor imaging of acute mild traumatic brain injury in adolescents. *Neurology*, **70**(12), 948–955.

Winkler, A. M., Ridgway, G. R., Webster, M. A., Smith, S. M., and Nichols, T. E. (2014). Permutation inference for the general linear model. *Neuroimage*, **92**, 381–397.

Zhang, K., Johnson, B., Gay, M., Horovitz, S. G., Hallett, M., Sebastianelli, W., and Slobounov, S. (2012). Default mode network in concussed individuals in response to the ymca physical stress test. *Journal of neurotrauma*, **29**(5), 756–765.

Zhang, Y., Brady, M., and Smith, S. (2001). Segmentation of brain mr images through a hidden markov random field model and the expectation-maximization algorithm. *IEEE transactions on medical imaging*, **20**(1), 45–57.

Zhu, D. C., Covassin, T., Nogle, S., Doyle, S., Russell, D., Pearson, R. L., Monroe, J., Liszewski, C. M., DeMarco, J. K., and Kaufman, D. I. (2015). A potential biomarker in sports-related concussion: brain functional connectivity alteration of the default-mode network measured with longitudinal resting-state fmri over thirty days. *Journal of neurotrauma*, **32**(5), 327–341.